NAVAL POSTGRADUATE SCHOOL
Monterey, California

THESIS

W222828

BANDWIDTH AND SIGNAL-TO-NOISE RATIO
ENHANCEMENT OF THE NPS TRANSIENT
ELECTROMAGNETIC SCATTERING LABORATORY

by

Norman J. Walsh

December 1989

Thesis Advisor: Michael A Morgan

REPORT DOCUMENTATION PAGE

1. REPORT SECURITY CLASSIFICATION UNCLASSIFIED		1b RESTRICTIVE MARKINGS		
2. SECURITY CLASSIFICATION AUTHORITY		3 DISTRIBUTION/AVAILABILITY OF REPORT Approved for public release; distribution is unlimited		
2b DECLASSIFICATION/DOWNGRADING SCHEDULE				
4 PERFORMING ORGANIZATION REPORT NUMBER(S)		5 MONITORING ORGANIZATION REPORT NUMBER(S)		
6a NAME OF PERFORMING ORGANIZATION Naval Postgraduate School	6b OFFICE SYMBOL (If applicable) 62	7a NAME OF MONITORING ORGANIZATION Naval Postgraduate School		
6c ADDRESS (City, State, and ZIP Code) Monterey, California 93943-5000		7b. ADDRESS (City, State, and ZIP Code) Monterey, California 93943-5000		
8a NAME OF FUNDING SPONSORING ORGANIZATION	8b OFFICE SYMBOL (If applicable)	9 PROCUREMENT INSTRUMENT IDENTIFICATION NUMBER		
8c ADDRESS (City State and ZIP Code)		10 SOURCE OF FUNDING NUMBERS		

PROGRAM ELEMENT NO	PROJECT NO	TASK NO	WORK UNIT ACCESSION NO

11. TITLE (include Security Classification) BANDWIDTH AND SIGNAL-TO-NOISE RATIO ENHACEMENT OF THE NPS TRANSIENT ELECTROMAGNETIC SCATTERING LABORATORY

12. PERSONAL AUTHOR(S)
WALSH, Norman J.

13a TYPE OF REPORT Master's Thesis	13b TIME COVERED FROM ____ TO ____	14 DATE OF REPORT (Year, Month, Day) 1989 December	15 PAGE COUNT 76

16 SUPPLEMENTARY NOTATION The views expressed in this thesis are those of the author and do not reflect the official policy and position of the Department of Defense or the US Government.

17 COSATI CODES			18 SUBJECT TERMS (Continue on reverse if necessary and identify by block number)
FIELD	GROUP	SUB-GROUP	Radar Cross Section; Transient Scattering, Signature

19 ABSTRACT (Continue on reverse if necessary and identify by block number)

This thesis describes the development of a parallel GaAs FET amplifier configuration for the Transient Electromagnetic Scattering Range at the Naval Postgraduate School. The implementation of the parallel amplifier configuration improved the bandwidth and the signal-to-noise ratio of the range. Existing software was used to process signals scattered from canonical targets. When interpreted, this data was used to optimize the new amplifier configuration. The upgraded facility is shown to provide measurements having excellent agreement with theoretically predicted signatures of simple canonical shapes. A significant improvement of the signal-to-noise ratio and bandwidth of scattered signature vis-a-vis that of the previous laboratory configuration is observed. Results are documented for a target library created to facilitate research into a number of scattering problems.

20 DISTRIBUTION/AVAILABILITY OF ABSTRACT ☒ UNCLASSIFIED/UNLIMITED ☐ SAME AS RPT ☐ DTIC USERS	21. ABSTRACT SECURITY CLASSIFICATION UNCLASSIFIED	
22a NAME OF RESPONSIBLE INDIVIDUAL MORGAN, Michael A.	22b TELEPHONE (Include Area Code) 408-646-2677	22c OFFICE SYMBOL 62Mw

DD FORM 1473, 84 MAR

83 APR edition may be used until exhausted
All other editions are obsolete

SECURITY CLASSIFICATION OF THIS PAGE

UNCLASSIFIED

BANDWIDTH AND SIGNAL-TO-NOISE RATIO ENHANCEMENT OF THE NPS
TRANSIENT ELECTROMAGNETIC SCATTERING LABORATORY

by

Norman J. Walsh
Major, Royal Canadian Armored Corps
B.S.C., Royal Military College of Canada, 1975

Submitted in partial fulfillment
for the degree

MASTER OF SCIENCE IN ELECTRICAL ENGINEERING
December 1989

NAVAL POSTGRADUATE SCHOOL
Monterey, California

ABSTRACT

This thesis decribes the development of a parallel GaAs
FET amplifier configuration for the Transient Electro-
magnetic Scattering Range at the Naval Postgraduate School.
The implementation of the parallel amplifier configuration
improved the bandwidth and the signal-to-noise ratio of the
range.   Existing software was used to process signals
scattered from canonical targets.   When interpreted, this
data was used to optimize the new amplifier configuration.
The upgraded facility is shown to provide measurements
having excellent agreement with theoretically-predicted
signatures of simple canonical shapes.   A significant
improvement of the signal-to-noise ratio and bandwidth of
scattered signatures vis-a-vis that of the previous
laboratory configuration is observed.   Results are
documented for a target library created to facilitate
research into a number of scattering problems.

TABLE OF CONTENTS

.

LIST OF TABLES

LIST OF FIGURES

ACKNOWLEDGMENTS

I would like to thank Professor Michael A. Morgan, whose patience, tutoring and direction was instrumental to this work. Also, thanks are due to Paul Buczynski for manufacturing the numerous delay lines used in this endeavor.

This Thesis is dedicated to my children, Julie and David who tolerated their Daddy's idiosyncrasies over the course of this work. To Linda, my wife, who kept the home fires burning, I am forever grateful.

I. INTRODUCTION

A. BACKGROUND

Electromagnetic analysis and design have tended to be historically-based on frequency domain techniques. In this domain the impulse response of a target is obtained by using a continuous wave (CW) system to sweep frequencies over the entire band of interest. Time-domain transient scattering measurements offer a faster, less expensive and more directly observable alternative. Made possible by the advent of fast pulse sources and sampling oscilloscopes, time domain techniques use direct pulse excitation to obtain the transient scattering response of a target.

The original Transient Electromagnetic Scattering Laboratory (TESL) at the Naval Postgraduate School (NPS) was an outside ground-plane range [Ref. 1]. This facility, initiated in 1980, was limited to symmetric targets due to the requirement for "mirror imaging". In 1983, an indoor facility became operational [Ref. 2]. This new facility used a shielded anecholic chamber, which eliminated the restriction to symmetrical targets as the target was, in effect, suspended within the chamber.

The TESL facilitated research into radar target identification using complex pole natural resonances. The transient scattering measurements and signal processing were

1

originally done using a Tektronix hardware setup. McDaniel
[Ref. 3] showed good agreement between the measurement of
impulse responses for a sphere and a thin wire.

Prior to the current effort, Sompaee [Ref. 4] designed
and implemented new software for experimental measurement
control and subsequent signal processing of transient
signatures to synthesize scattering impulse responses of
scale model targets. In addition, the TESL hardware was
upgraded to improve signal-to-noise ratio. Automatic
transient scattering measurements were obtained using an
IEEE bus controller, an IBM PC and a state-of-the-art
digital programmable oscilloscope (DPO).

Sompaee obtained good agreement between experimental
measurements and computations for simple canonical targets.
His noise analysis showed a 10 dB improvement over the
Tektronix hardware that was used before the upgrade of the
TESL.

B. OVERVIEW

The main objective of this research was to incorporate
two parallel GaAs FET broadband amplifiers to extend the
frequency range and further improve the signal-to-noise
ratio (SNR) of the TESL. The hardware layout was optimized
and the previously existing flexible coax cabling was

replaced with minimum length hard coax, given the restrictions of the existing structure of the chamber.

Validation of the improved facility was done by again comparing experimental results to those theoretically predicted for simple canonical targets. A library of high fidelity measurements for simple shapes and scale model military targets was created. This library is for use in the development of new natural resonance extraction algorithms and resonance annihilation filters for aspect invariant radar target identification.

This thesis is broken into seven chapters. Chapter II describes the TESL and the hardware changes incorporated as part of this thesis. The development of the new amplifier configuration is summarized.

Chapter III presents the theory of transient scattering measurements. Major time domain facility considerations are briefly discussed and the system frequency-domain represent-ation, with its mathematical model and transient response solution, are presented.

Chapter IV briefly reviews the acquisition algorithms and signal processing developed by Sompaee. It highlights how experimental measurements, once processed, were used in the development of the amplifier configuration discussed in Chapter II.

Chapter V discusses the experimental results that were used to validate the final configuration of the upgraded facility. Both sphere and thin wire scattering measurements are shown to have excellent agreement with theoretical predictions.

Chapter VI summarizes the target library created. Example results from scale model targets are presented.

Chapter VII summarizes all work and suggests some possible continuing research applications.

II. CHANGES IMPLEMENTED IN THE NPS TESL

A. LABORATORY DESCRIPTION

The NPS TESL is located in room 535 of Spanagal Hall. A general layout is depicted in Figure 1. The range incorporates a metallically shielded anechoic chamber, 6.2 m long by 3.1 m square. Targets were mounted on a low density styrofoam pedestal, 2.18 meters from the frontal plane of the antenna for this thesis work. The back wall of the chamber is covered with 46 cm long pyramids while the source wall is covered with 21 cm long pyramids. Sides, floor and ceiling are covered with longitudinal wedges to direct energy towards the absorbing back wall. The interior of this chamber, looking towards the source wall, is illustrated in Figure 2. Further details of the chamber can be found in References 2 and 3.

Details of the target acquisition hardware and software can be found in Reference 4. As part of this effort the following hardware was added to the facility:

- Midisco inductive power splitter;

- AVANTEK APT-12066 six-to-twelve GHz amplifier;

- HP 8349A microwave amplifier;

- Hard 141 mil coax cabling;

- Two cooling fans;

- One additional horn antenna; and

- Abacus 25 MHz Cache Memory 80386 Computer with 80387 and Weitek 3167 Coprocessors
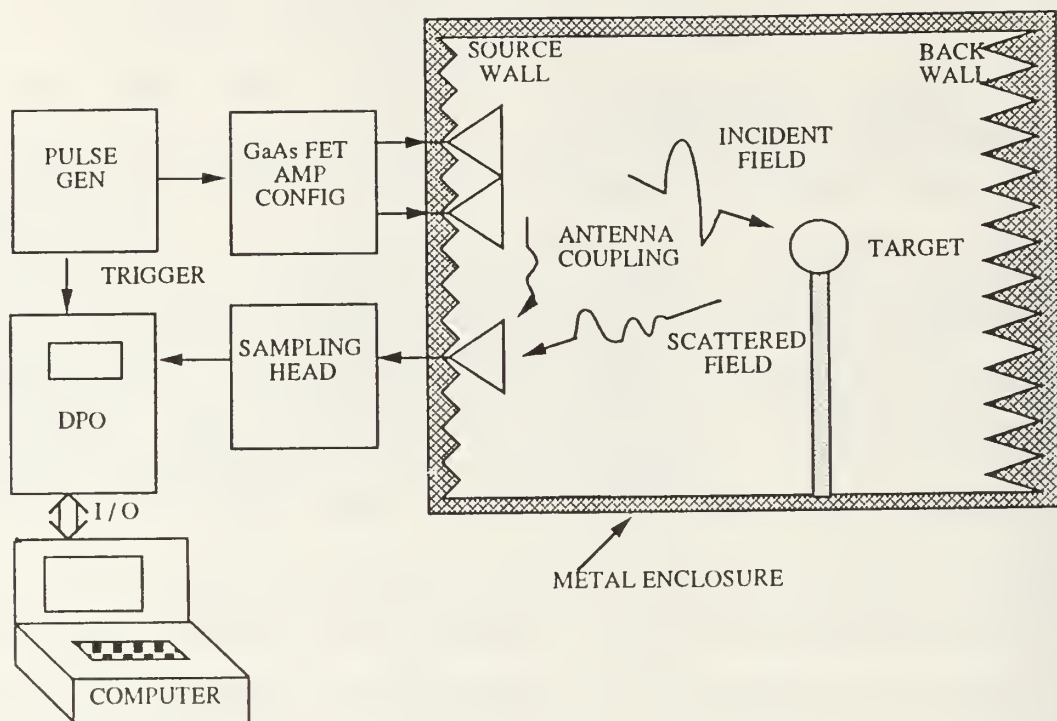
Figure 1.   NPS TESL general layout

B.   ANTENNA ARRAY

A 24-inch-square detachable panel was available in the center of the source wall of the chamber for mounting the antenna array. Two antennas, one transmitting and one receiving, were previously used. A new panel for mounting three antennas was needed. Since it was not practical to mount all three antennas in a line, the two transmitting antennas were mounted above the center line of the panel and the receiving antenna below. The three antennas were mounted

6
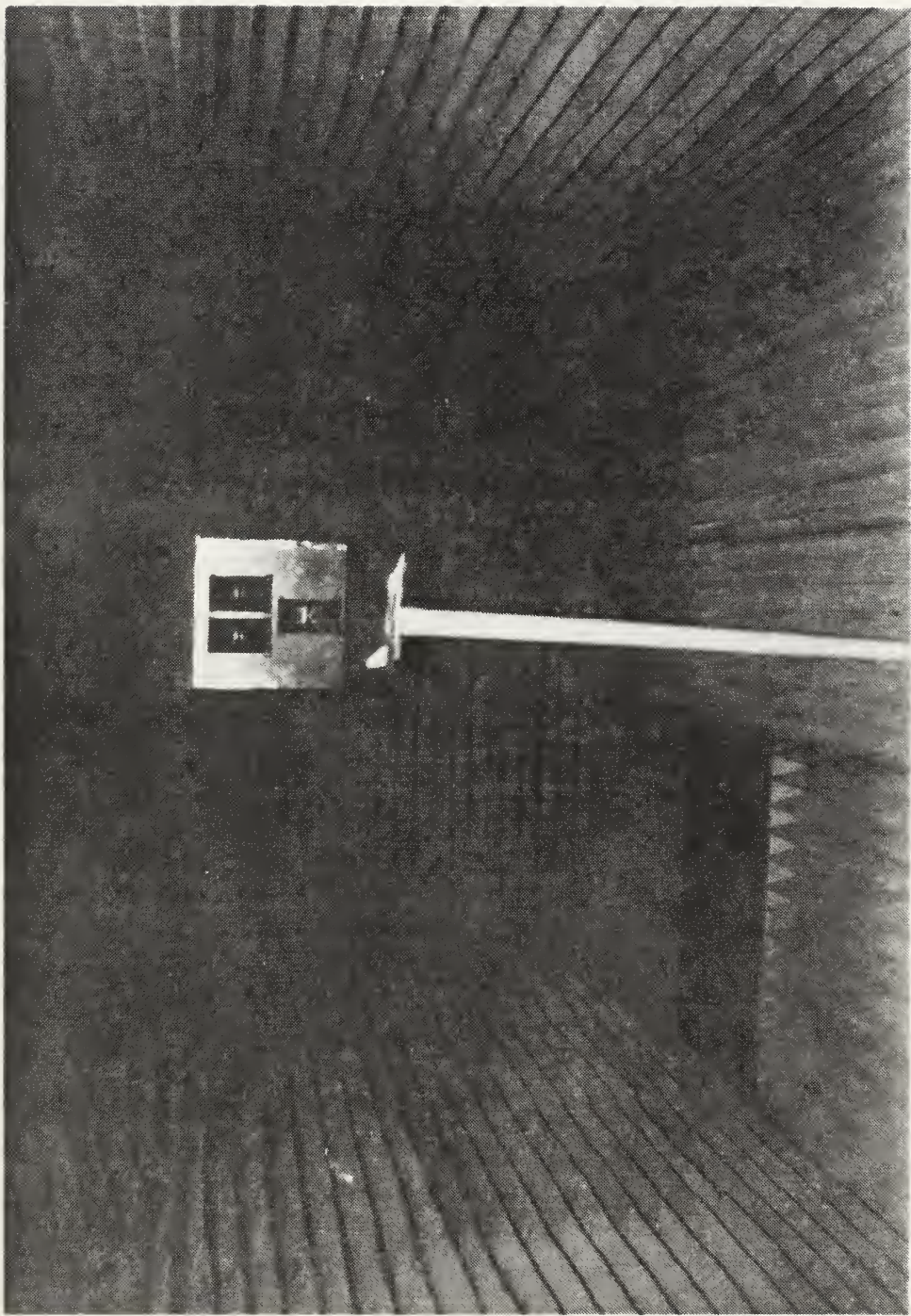
Figure 2.   Interior of anechoic chamber

7

to be symmetrical about the center of the panel, as can be seen in Figure 3. The antennas were then shimmed to point to the position in space where the targets are mounted, at a distance of 2.18 meters from their face. As will be explained in Chapter IV, the metalized mounting panel was shielded with the same absorbing material as the source wall to eliminate any multi-path effects between the target and the mounting panel. Figure 4 shows how the antenna mounting panel was masked.

A shelf was constructed on the exterior of the antenna mounting panel in order to mount the amplifiers in close proximity to the transmitting antennas. The amplifier configuration is depicted in Figure 5. The evolution of this configuration is explained in the following sections. Figure 6 shows the general exterior equipment layout.

C. AMPLIFIER CHARACTERIZATION

The first step in the development of the parallel amplifier configuration was the characterization of the new 6-12 GHz GaAs FET unit. The manufacturer's guaranteed specifications for the Avantek APT-12066, one watt 6-12 GHz amplifier are listed in Table 1. The device was first mounted in a modified heat sink of unknown origin. As the device was too wide to fit into the heat sink, the two innermost fins were milled out. The heat sink was fitted to
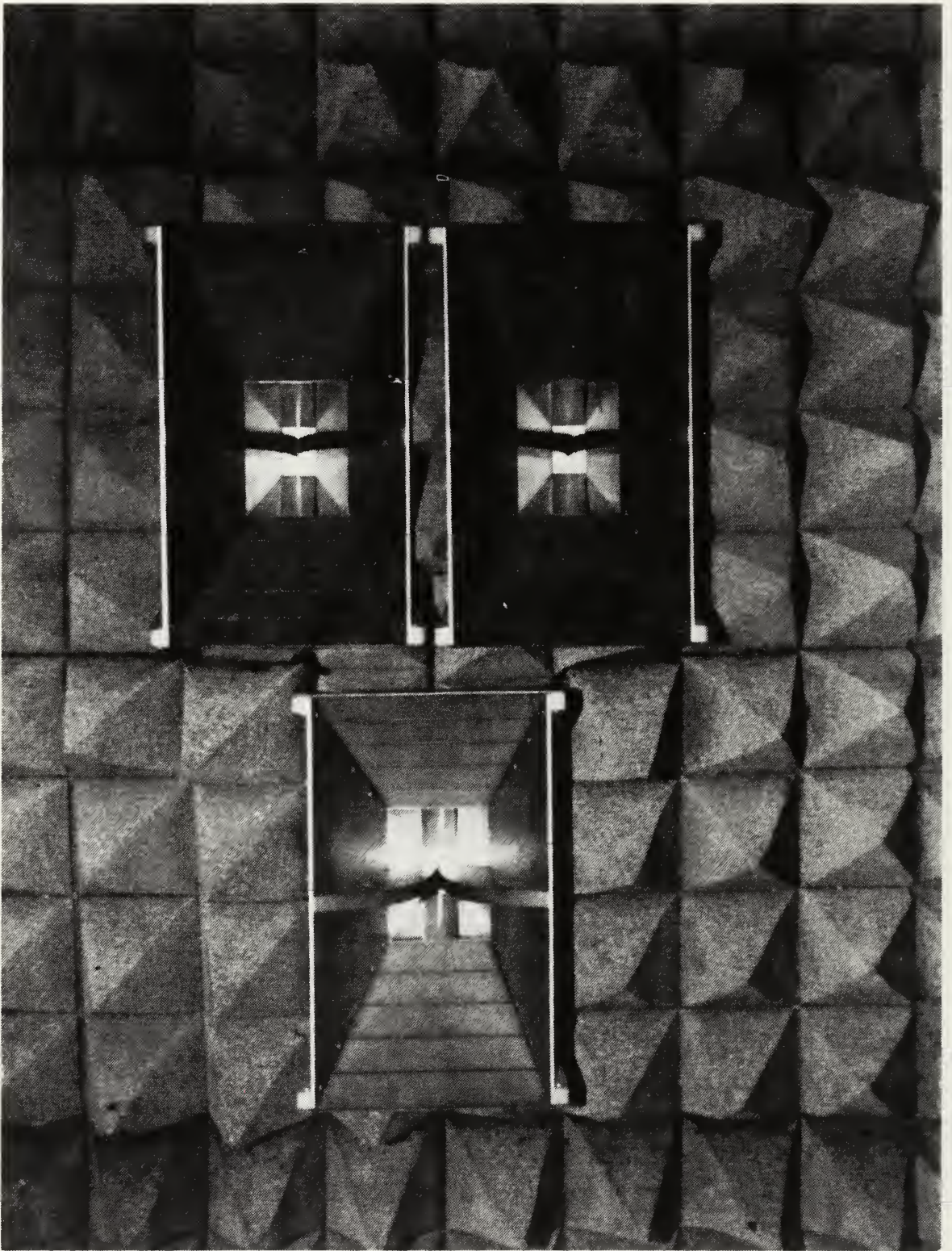
Figure 3.   Antennas mounted symmetrically

Figure 4.   Masking of antenna mounting panel

10
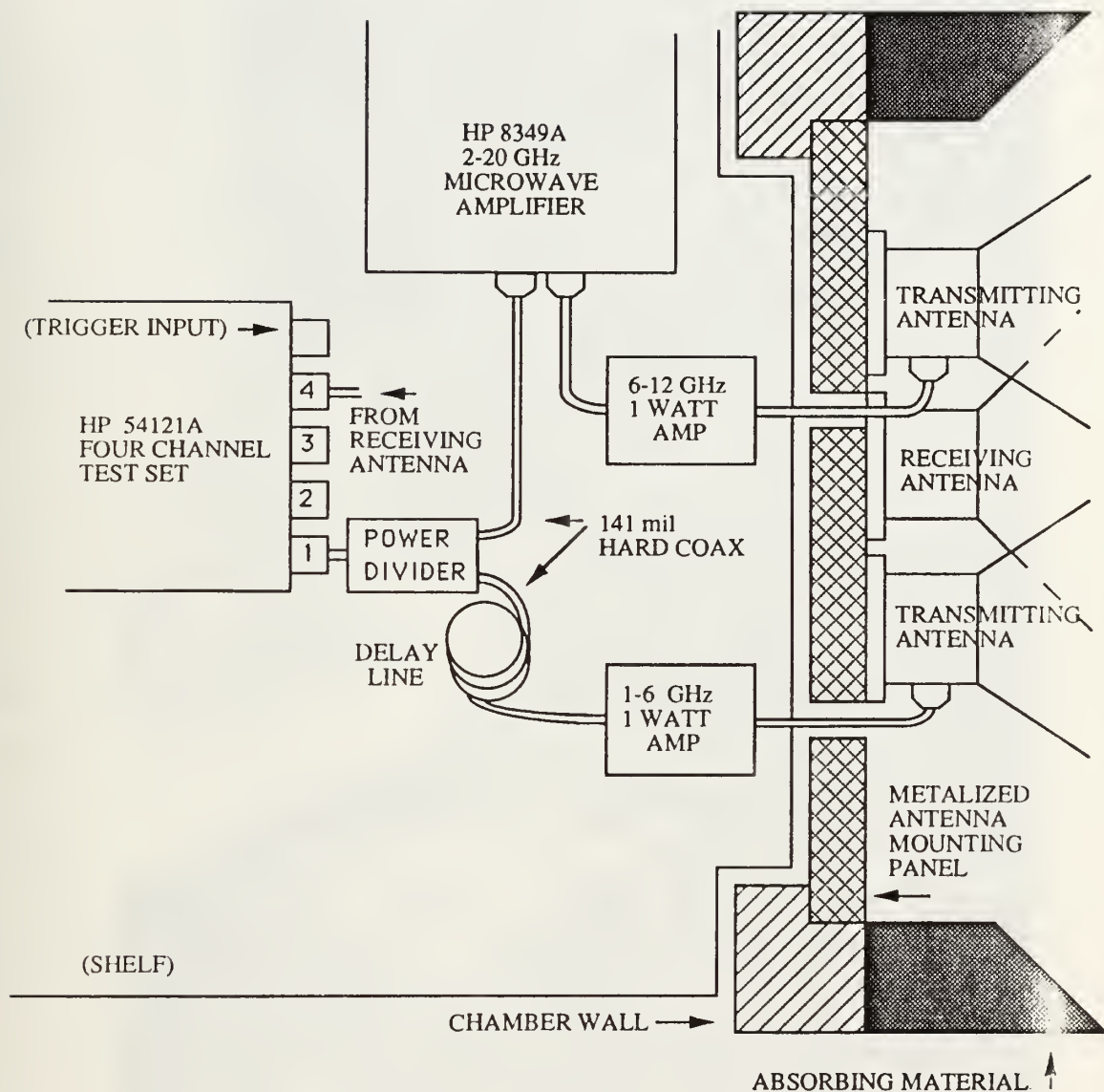
Figure 5.   Pre-amplifier/amplifier/delay line/antenna
            configuration

11
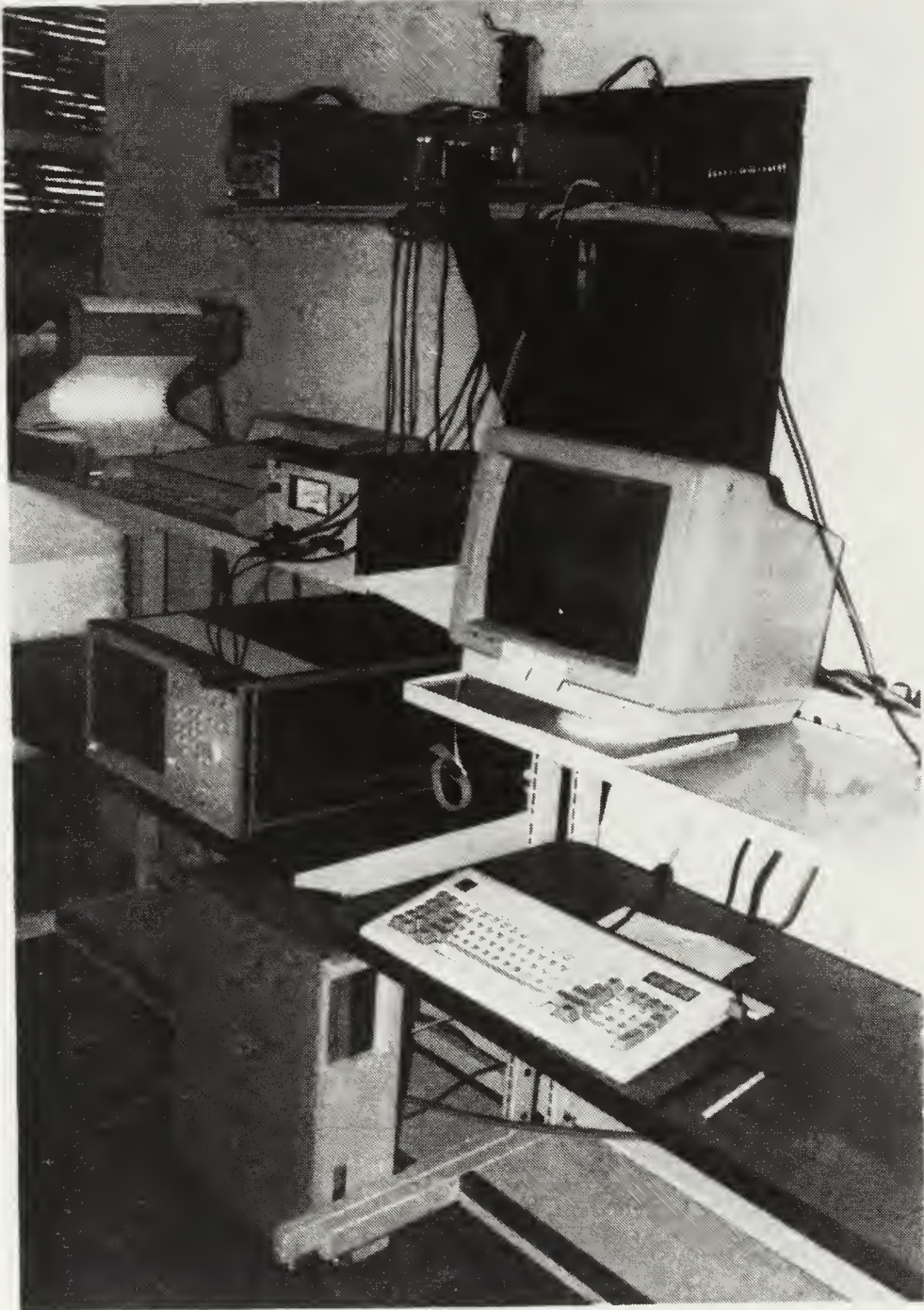
Figure 6.   Chamber exterior equipment layout

12

the length of the device, 7.5 cm. The amplifier was mated to the heat sink using type 120 thermal joint compound (EG&E Wakefield Engineering). The modified heat sink, with amplifier mounted, is illustrated in Figure 7.

TABLE 1. MANUFACTURER'S SPECIFICATIONS FOR NEW AMPLIFIER

Model	Frequency Response (GHz) Min.	Gain (dB) Min.	Gain (dB) Max.	Noise Figure (db) Max.	Power Output (Watts) Min.	Gain Flatness (+/-dB) Max.
APT-12066	6-12	28	39	8.0	1.0	1.5

The characterization of the amplifier was done using an HP 8756A Scalar Network Analyzer and 8350B Sweep Oscillator. This was performed in three stages: low input power, medium input power and a full specified power test. In all three stages, a -20dB HP 33340C attenuator was mounted on the output port of the amplifier to protect the HP 11664A detector used with the network analyzer. The device was also investigated using a bias voltage of less than the specified + 15 volts dc. During testing the device case temperature was monitored with a Fluke 80T-150 temperature probe and HP 3469B multimeter.
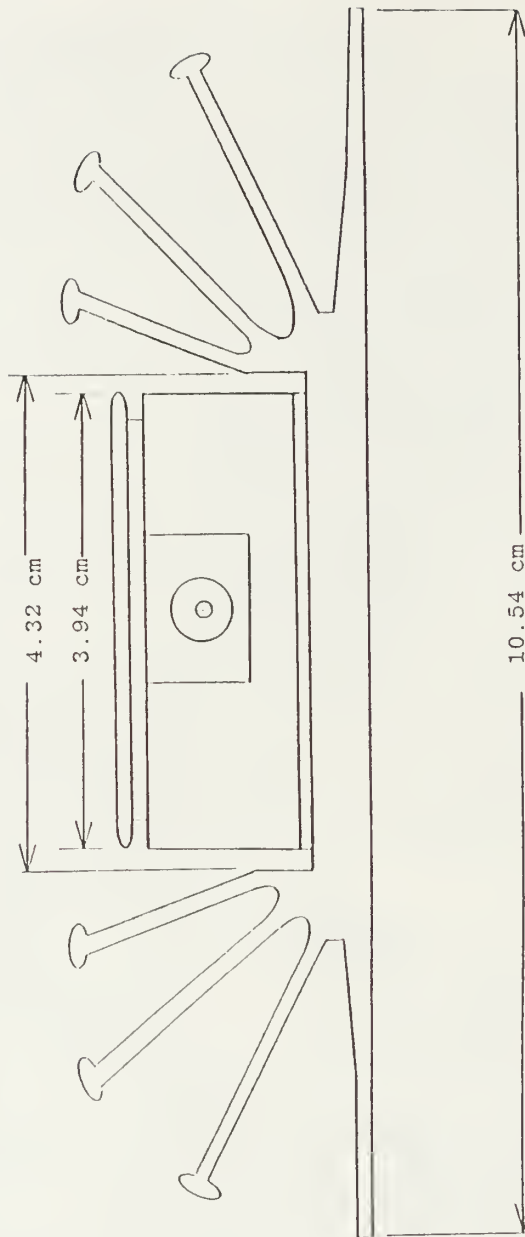
Figure 7.   Amplifier mounting in heat sink

At low input power (-30 dBm) it became apparent that the the heat sinking described above was inadequate as the measured case temperature rose above the specified maximum (50 C) after approximately one hour. The device performance remained within specification until the case temperature rose above 55 C. The bias voltage was decreased to +12 volts DC and the case temperature stabilized at 78.4 C. At this case temperature the average gain across 6-12 GHz was less than 26 dB. At a bias voltage of + 15 volts the temperature rose above 100 C and did not stabilize. At this point the test was terminated for fear of damaging the device.

Once a small fan was positioned to blow over the amplifier the case temperature stabilized at approximately 41 C, and this temperature did not vary measurably between an input power of -20 or -10 dBm. The device gain remained stable at roughly +31 dB across the 6-12 GHz bandwidth. A response peak of 33.05 dB was noted at 11.1 +/- 0.05 GHz.

No measurable difference in the output of the device was found when it was biased between +13 and +15 Volts DC. Similar results were obtained when confirming the characteristics of the 1-6 GHz device [Ref. 4]. For all of this work both devices were operated with a bias voltage of +13 volts DC to keep the case temperatures within the manufacturer's specification. With the two personal computer-type cooling fans used in the final configuration

it was found that the device temperature would approach 50 C if the room temperature rose above 22 C when biased at +15 Volts. When biased at +13 C the device temperature would stabilize at approximately 44 C with an ambient room temperature of 22 C.

To confirm the device reliability an eight-hour full-power test was then conducted. The input power was set at -2 dBm and the average device response was greater than +31 dB. The ambient room temperature at the start of test was + 17.9 C and rose to + 22.2 C by day's end. The device response was measured periodically throughout the day at 6, 8, 10, and 12 GHz, as well as the peak amplification frequency of 11.1 +/-

of test, the amplifier took approximately one and one-half hours to reach a stable temperature. The output of the APT-12066 at the end of this test is illustrated in Figure 8.

D. PRE-AMPLICICATION AND DELAY LINE

The initial concept for the implementation of the parallel amplifiers was to take the output from the pulse generator through an inductive power splitter, directly into the two GaAs FET amplifiers and on into the transmitting antenna, using the minimum possible lengths of hard coax. When this was set up on a test bench and fed directly back into the sampling head through 40 dB of attenuation, it was

TABLE 2. FULL POWER TEST RESULTS

Time	Case Temp. C	GAIN			
		6 GHz dB	8 GHz dB	10 GHz dB	12 GHz dB
0830	34.0	31.39	30.95	31.45	30.64
1005	40.9	30.95	30.97	31.48	30.40
1105	42.1	30.90	30.96	31.97	30.37
1230	40.8	30.96	30.96	31 47	30.39
1330	42.8	30.91	30.96	31,46	30.36
1500	43.6	30.87	30.96	31.46	30.35
1625	42.9	30.88	30.95	31.47	30 36

found that the the magnitude of the 6-12 GHz pulse was app-
roximately one-fifth of the 1-6 GHz pulse. Spectral invest-
igation and simple modeling of the 25 psec rise time step
pulse from the DPO confirmed this order of magnitude diff-
erence in the spectral distribution over the 1-6 versus 6-12
GHz spectrum. This amplitude difference can be seen in an
example measurement from the bench testing in Figure 9.
Figure 9 was plotted directly from the DPO.   The peak
amplitude of the 6-12 GHz pulse is roughly 12 mVolts.   The
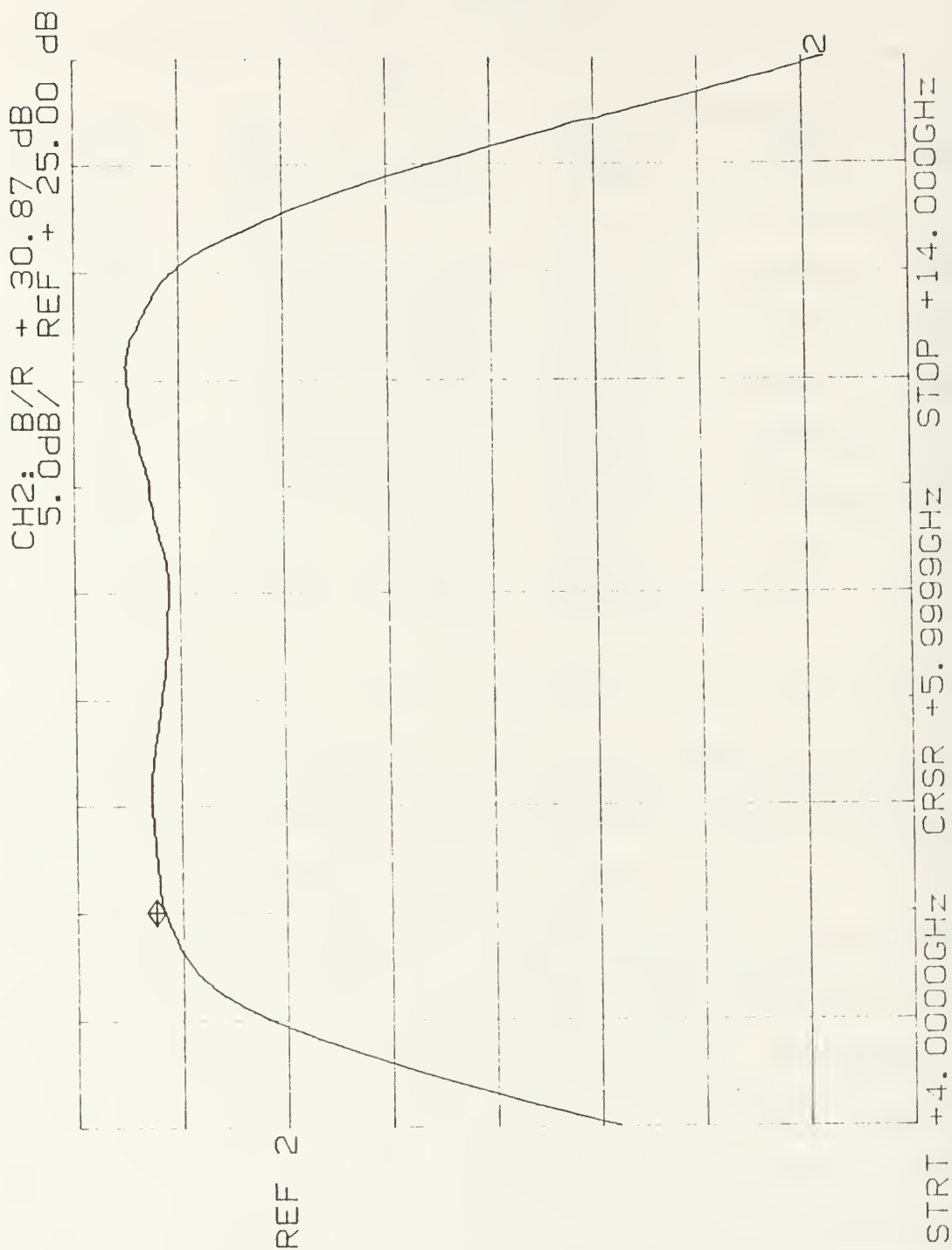peak amplitute of 1-6 GHz pulse is approximately 60 mVolts.

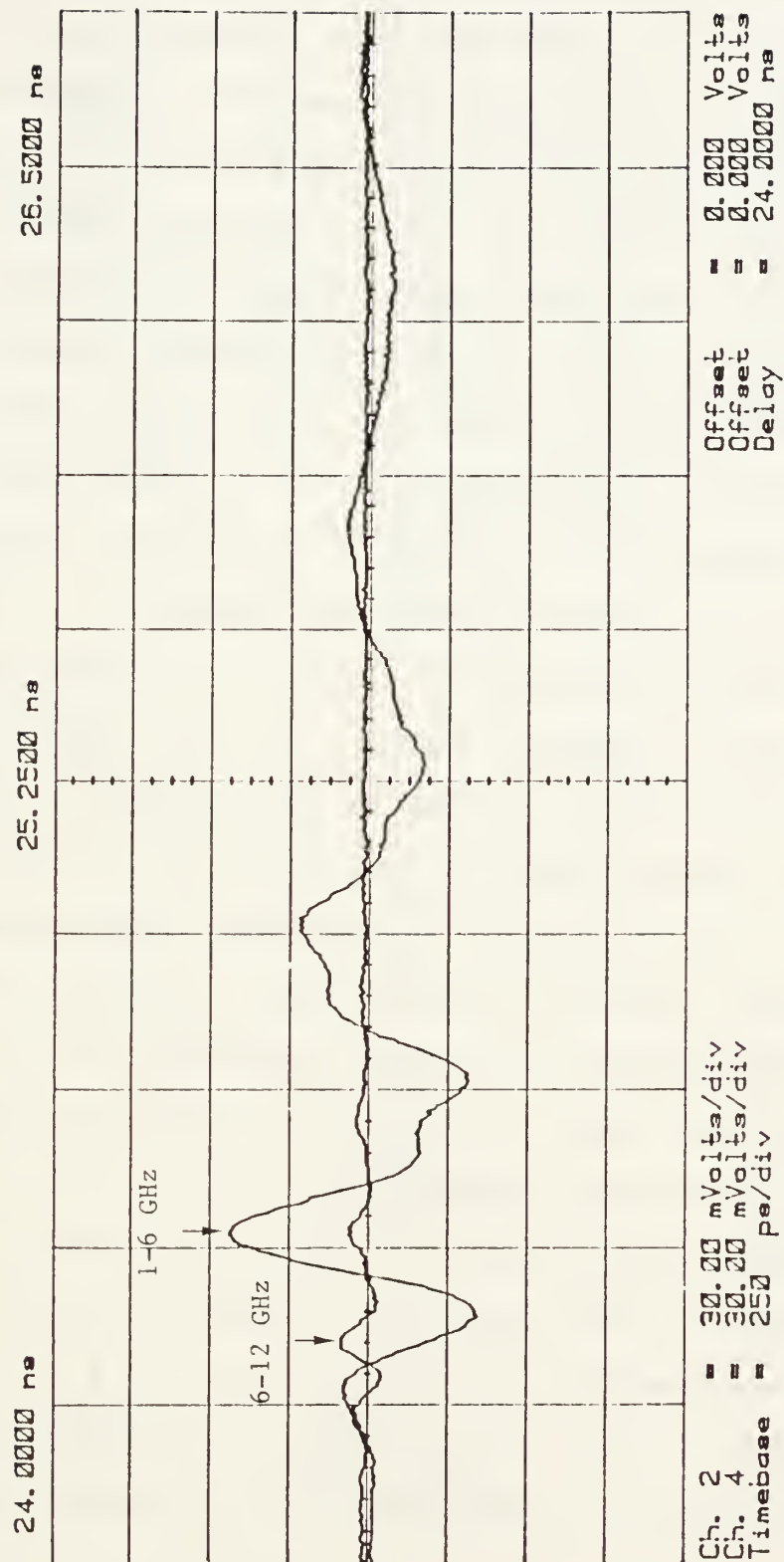Figure 8.   Amplifier spectral response

18

Figure 9.   Return signal without pre-amplification

19

This amplitude difference was clearly undesirable, given the objective of improving the bandwidth and SNR of the TESL. The APT-12066 Amplifier was the highest gain 1 watt 6-12 GHz amplifier available when purchased. It was decided to use an available HP 8349A microwave amplifier to pre-amplify the 6-12 GHz pulse. Using the minimum possible lengths of hard coax, given the physical chamber structure, equipment size and need for air circulation, the pre-amplification introduced a 3.95 +/- 0.1 ns delay in the 6-12 GHz pulse. This time delay can be seen in Figure 10.

When this pre-amplifier configuration was implemented, with sample measurements taken and processed, (to be described in Chapter Three), it was observed that deep "valleys" or holes existed in the spectrum in the area of spectral overlap between the amplifiers. This observation lead to the conclusion of destructive interference between the pulses, possibly because of the time delay introduced by pre-amplification. It was then decided to delay the 1-6 GHz pulse so that the scattered signals arrived at the receiving antenna simultaneously.

To determine the delay necessary a number of scattering measurements were made and averaged. The implication of these measurement was that a 3.95 +/- 0.1 ns delay was required. The +/- 0.1 ns delay was not resolvable by the visual images on the monitor or printer being used.

20

Figure 10.   Return signal with pre-amplification

21

Inherent noise made it it difficult to measure (or to determine on a hard copy) the exact location of the subjective front edge of a scattered pulse.

There was also some uncertainty as to the effect of the dielectric fill in the hard coax cable being used. The dielectric constant for polytetrafluoroethylene (Teflon) found in handbooks [References 5, 6 & 7] varied from 2.08 to 2.1. It is suspected that some variance with frequency over 1-12 GHz exists but no supporting literature was found. Using formula 2.1 and the manufacturer-specified inner radius ("a"), outer radius ("b") and characteristic impedance ("Z_o") [Ref. 8] one calculates a dielectric constant of 2.0006. [Ref. 9]

$$Z_0 = \frac{1}{2\pi} \sqrt{\mu/\varepsilon} \ \ln(b/a) \quad\quad\quad (2.1)$$

Given the uncertainty in ε it was determined that the length of delay line needed was 84 +/- 2 cm, in addition to the 11.2 cm feed line used when the measurements were made.

A number of delay lines were manufactured, varying from 76 to 102 cm in length. Each was used for a series of measurements and the resulting data was processed using a deconvolution algorithm and an FFT plotting package [Ref. 10]. The results were examined for completeness of their spectrum and for evidence of interference in the amplifier

22

spectral overlap area. It was found that delay lines measuring from 92.71 to 99 cm gave good results. The best results were obtained using a 97.8 cm delay line. A typical scattered signal, obtained using the 97.8 cm delay line configuration, is shown in Figure 11. The final delay line can be seen in Figure 12.
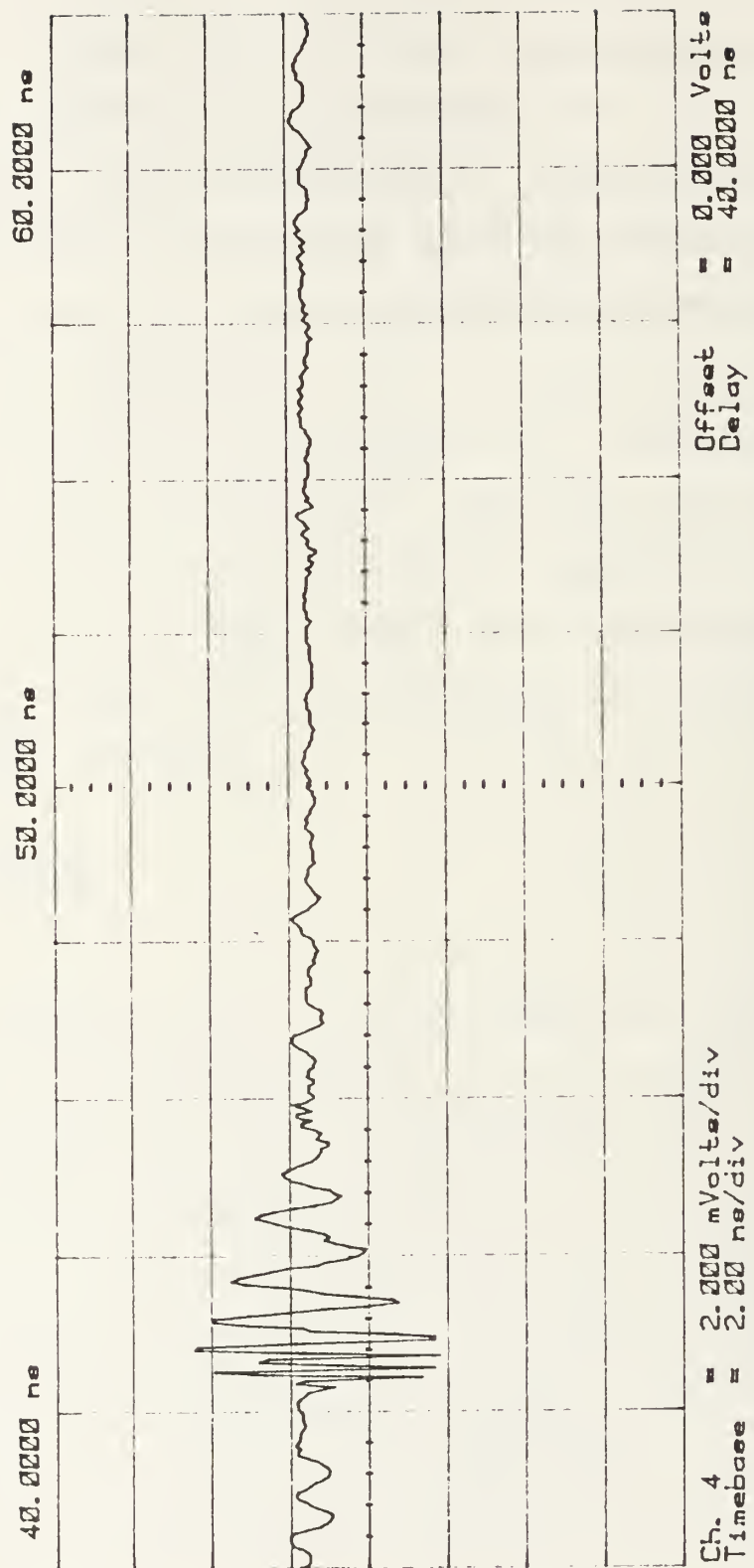
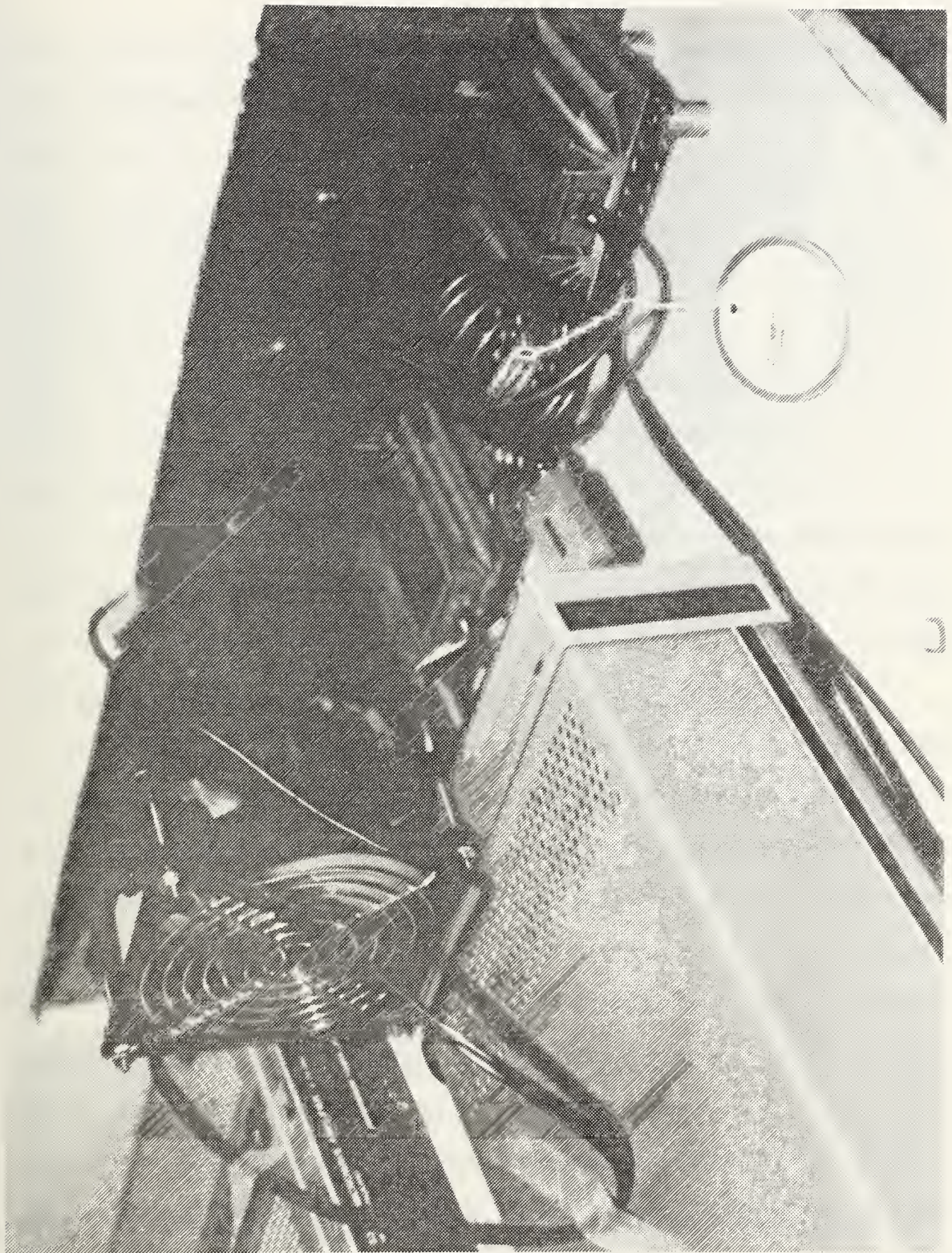Figure 11.   Return signal with pre-amplification
and delay line

24

Figure 12.   Implementation of 97.8 cm delay line

III. THEORY OF TRANSIENT SCATTERING MEASUREMENTS

A. TIME DOMAIN SCATTERING MEASUREMENTS

Transient electromagnetic scattering measurements can, in essence, be considered an extension of Time Domain Refectometry (TDR). In the TESL, the TDR pulse source is available from channel 1 of the four-channel test set (HP 54121A), a sub-assembly of the DPO. This sub-assembly also acts as the trigger for the DPO sampling circuits. The rise time of the step generator is approximately 25 psec and, for this work, was operated at a pulse repetition rate of 500 kHz.

The target acquisition algorithm [Ref. 4] is set up so that the number of data points in a time series has to be a power of 2. Ensemble waveform averaging increases power or energy SNR by the number of averages, N. For this work 1024 data points were acquired in a 20 ns window, averaged 2048 times.

The close proximity of the transmitting and receiving antennas results in a very large direct coupling of energy into the receiving antenna. As the pulse exits the transmitting antennas this direct-coupled energy is many orders of magnitude larger than most transient target responses. If both were recorded, the desired response would be unobservable using the required visual scale factors.

26

This potential problem is avoided by setting the delay between the pulse generation and the start of the return sampling so as to time window the transient target response. With the new amplifier configuration this delay was 40 nsec. By that time the residual "ringing" between the antennas was much smaller than the target response and, as will be explained in the following sections, was subtracted out in the post-processing.

B.   TESL SYSTEM REPRESENTATION

A free-field scattering range system representation is shown in Figure 13. The interactions in the scattering process within the system are represented by frequency domain transfer functions.

The amplified pulse generator output, $X(f)$, drives the transmitting antennas whose combined transfer function is denoted by $H_T(f)$. The transmitted field immediately couples into the receiving antenna, $H_A(f)$, which, in turn, interacts with the scatterer, $H_S(f)$, and the absorbing material in the chamber, $H_C(f)$. The mutual interaction between the scatterer and the chamber walls is denoted by the two-way arrow, $H_C(f)$ to $H_S(f)$. The effects from all these sources are summed in the receiving antenna, whose transfer function is $H_R(f)$. Noise is added to the system from thermal emissions within
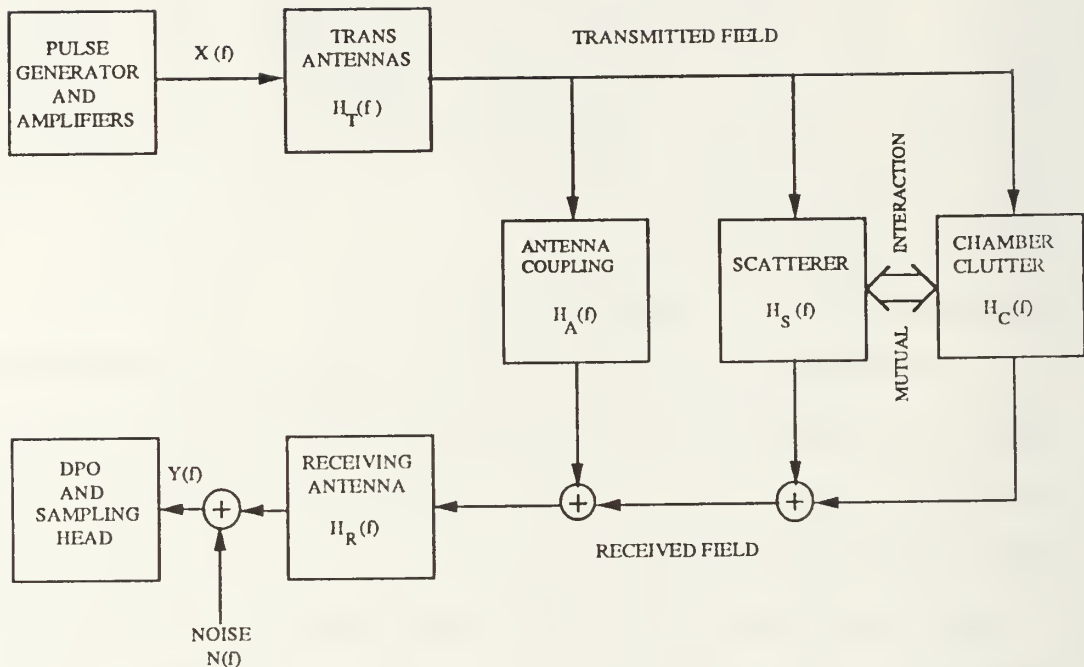
Figure 13. TESL system representation

the chamber and from the sampling front end of the DPO. Total noise is denoted N(f). The net signal sampled by the DPO is denoted by Y(f).

To extract the target transfer function, $H_S(f)$, three separate measurements are required. The first is with no

target present and is termed the "background measurement". The second is with a target present, termed the "target measurement", and the transfer functions are denoted with a superscript "T". The third is with a canonical target, termed the "calibration measurement", and the transfer functions are denoted with a superscript "C". The following table summarizes the transfer functions used in the mathematical model developed in the following section.

TABLE 3. SYSTEM REPRESENTATION TRANSFER FUNCTIONS

Amplified pulse driving the antennas	$X(f)$
Transmitting antennas response	$H_T(f)$
Receiving antenna response	$H_R(f)$
Antenna coupling	$H_A(f)$
Target response	$H_S(f)$
Chamber response (clutter)	$H_C(f)$
Interaction between target and chamber (including multipath and multiple scattering)	$H_{SC}(f)$
Target response, target measurement	$H_S^T(f)$
Multiple scattering between target and absorber target measurement	$H_{SC}^T(f)$
Calibration sphere response, calibration measurement	$H_S^C(f)$
Multiple scattering between calibration sphere and absorber, calibration measurement	$H_{SC}^C(f)$
Total system noise	$N(f)$
Net signal which is sampled	$Y(f)$

C. MATHEMATICAL MODEL

Each of the three measurements described in Part III B can be expressed as a product and sum of their constituent transfer functions. The resultant signal spectrum at the sampling head for a background measurement will be given by

$$Y_1(f) = H_R(f) \; H_T(f) \; X(f) \; \{H_A(f) + H_C(f)\} + N_1(f) \qquad (3.1)$$

This equation states that the received response to the amplified signal is equal to the product of the driver and antenna transfer functions times the sum of the antenna coupling and chamber response. The system noise is added to this product. The following two equations are similar in form except that the target or calibration sphere response, and their applicable interaction with the chamber, are included in the sum. A target measurement is given as

$$Y_2(f) = H_A(f) \; H_T(f) \; X(f) \; \{H_A(f) + H_C(f) + H_S^T(f) + H_{SC}^T(f)\}$$
$$+ N_2(f)$$
$$(3.2)$$

A calibration measurement is given as

$$Y_3(f) = H_R(f) \; H_T(f) \; X(f) \; \{H_A(f) + H_C(f) + H_S^C(f) + H_{SC}^C(f)\}$$
$$+ N_3(f)$$
$$(3.3)$$

These three equations represent the transforms of the measurements obtained directly in the time domain. The post-

processing described in the next section leads to the extraction of the desired transient response.

D. TRANSIENT RESPONSE POST-PROCESSING

Deconvolution post-processing makes it possible to synthesize the transient scattering response of the measured target to any pre-defined incident field whose spectrum fits within the pass band of the measurement system. A double gaussian pulse was used as the specified excitation in the deconvolution process, as will be discussed shortly. With the implementation of the parallel amplifiers, the DPO, amplifier configuration and transmitting antennas are roughly matched in the pass band of 1-12.4 GHz.

To synthesize the target's transfer function, the first step is to subtract from the calibration and target measurements the chamber clutter and the antenna coupling. These are embodied in the background measurement, equation 3.1. The subtraction of equation 3.1 from 3.2 and from 3.3 leads to equations 3.4 and 3.5.

$$Y_4(f) = Y_2(f) - Y_1(f)$$
$$= H_T(f)\ H_R(f)\ X(f)\ \{H_S^T(f) + H_{SC}^T(f)\} + N_4(f) \qquad (3.4)$$

$$Y_5(f) = Y_3(f) - Y_1(f)$$
$$= H_T(f)\ H_R(f)\ X(f)\ \{H_S^S(f) + H_{SC}^S(f)\} + N_5(f) \qquad (3.5)$$

where $N_4(f)$ and $N_5(f)$ represent the difference in the noise part of the measurement between the background and the target and calibration measurements, respectively.

The difference of the time domain measurements represented by equations 3.4 and 3.5 are then transformed into the frequency domain by a fast Fourier transform (FFT). An optimal deconvolution estimator, developed by Riad [Ref. 11], is then formed:

$$X_0(f) \ H_S^T(f) = \frac{Y_4(f) \ Y_5^*(f)}{Y_5(f) \ Y_5^*(f) \ + \ C} \ (X_0(f) \ H_S^C(f)) \qquad (3.6)$$

The smoothing parameter "C", establishes a minimum for the denominator and prevents noise enhancement at frequencies where the spectrum of Y_5 approaches zero. The expression $(X_0(f) \ H_S^C(f))$ represents the computed calibration sphere and $X_0(f)$ is the Fourier transform of $x_0(t)$,

$$X_0(f) = \Im\{x_0(t)\} \qquad \text{(the specified incident pulse)} \qquad (3.7)$$

The double-gaussian pulse used in this work is specified by:

$$x_0(t) = c_1 \ e^{-\alpha_1(t-t_0)^2} + c_2 \ e^{-\alpha_2(t-t_0)^2} \qquad (3.8)$$

32

C_1 and C_2 are chosen such that

$$x_0(t_0) = 1 \qquad (3.9)$$

and

$$\int_{-\infty}^{+\infty} x(t)\, dt = 0 \qquad (3.10)$$

The double gaussian waveform of equation 3.8 will have two specified 10% pulse widths, Δt_K, such that

$$e^{\frac{-\alpha_k}{4}(\Delta t_k)^2} = 0.1 \quad \text{for} \quad k = 1, 2 \qquad (3.11)$$

It can be shown that the estimator of equation 3.6 provides the best least-squares fidelity for the deconvolved target response. Equation 3.6 represents the frequency domain scattering response for the specified incident pulse whose Fourier transform is $X_0(f)$. Two programs written by Morgan are used to numerically generate the theoretical response, $(X_0(f)\, H_S^C(f))$, of the calibration sphere [Ref. 2]. Called Mie and SPRSCT, the latter uses magnitude and phase data generated by a Mie series in the former to generate the transient response of the sphere due to the double gaussian incident pulse.

The subtraction and optimal deconvolution routines are part of the software developed by Sompaee [Ref. 4]. In the next chapter it will be shown how the results of these algorithms were used in the development of the amplifier configuration.

33

IV. POST-PROCESSING

A. DECONVOLUTION ALGORITHM

The subtraction and optimal deconvolution algorithm, as described mathematically in the previous chapter, are embedded in the TESL computer software support system. This program was originally written by Morgan for the first TESL Tektronics microcomputer [Ref. 2]. It was converted to Fortran 77 by Sompaee and installed in the microcomputer used in the TESL [Ref. 4]. The program has graphic capabilities and allows the operator to obtain a hard copy at each step of the deconvolution procedure. The data files used in all the TESL software support systems have a standardized format.

The program starts by asking the operator for the name of the file containing the theoretically computed transient scattering by the calibration sphere target. This file is produced by successive runs of two programs MIE.BAS and SPRSCT.FOR. After reading the file, the program displays the time-series plot of the theoretical scattering. The calibration sphere scattering is then transformed into the frequency domain and displayed so that the bandwidth can be checked. The bandwidth of the theoretical scattering obtained from the Mie series and SPRSCT programs must not exceed that of the measured data. Frequency and time-domain

plots for the 15.1 cm calibration sphere used in this work are shown in Figure 14.

The next step of the program is to read in the files for the measured calibration sphere and the measured background data. Both files are overlaid on the same axis and displayed to the operator. At this point the operator has the capability of shifting one of the waveforms to the left or right if he observes that time shifting has occurred. This capability was not found to be needed during this work. An example target and background measurement comparison is shown in Figure 15. The background waveform is then subtracted from the calibration measurement and the difference is transformed into the frequency domain.

The program then asks the operator for the target file name and its background file name. The operator has the option of using the background file subtracted from the calibration measurement or a different background file. In each case, over the course of this work, a background file was used which was obtained either immediately before or after the target measurement being processed. The program then follows the same procedure described for the calibration sphere: overlay, option to shift in time, subtraction and transformation. An example subtracted waveform is shown in Figure 16.

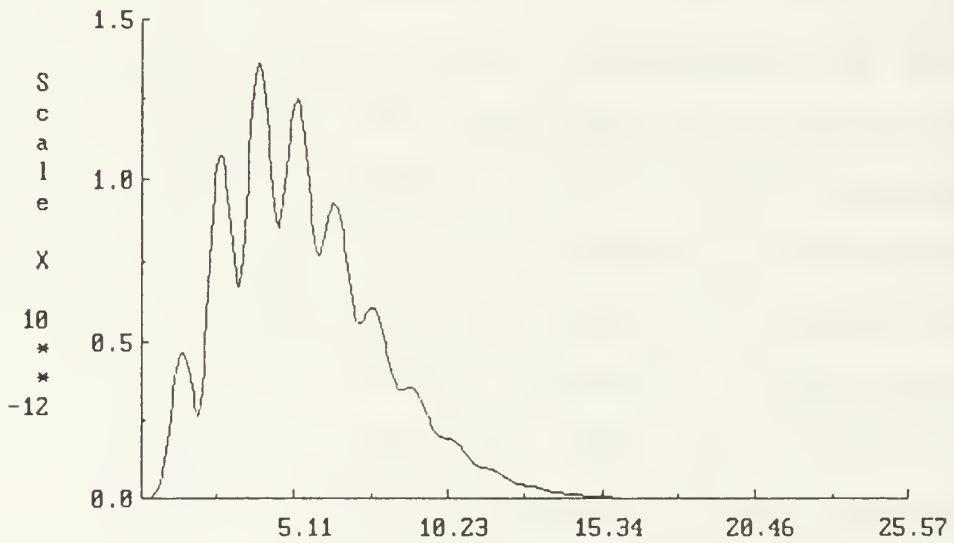Double Gaussian Pulse Transient Scattering
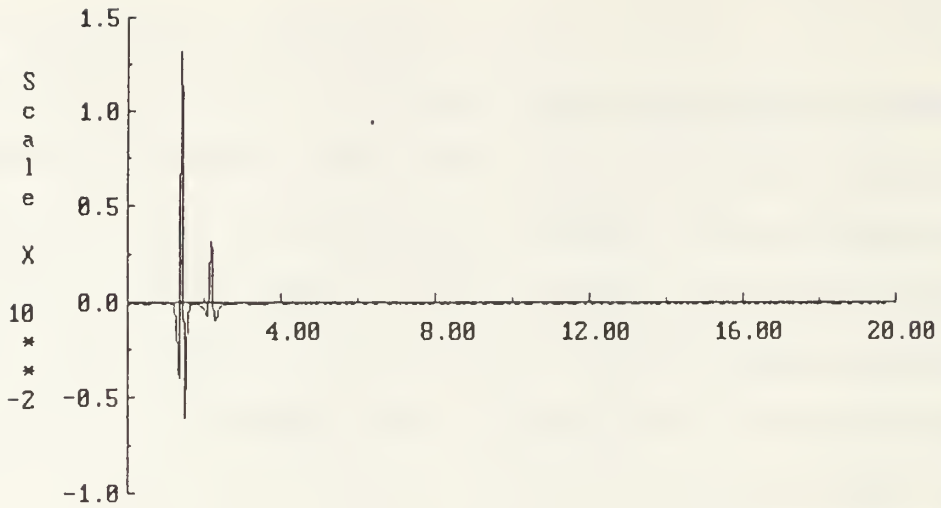
Spectral Magnitude of H(f)*P(f)

Figure 14. Time and frequency domain plots, theoretical
calibration sphere
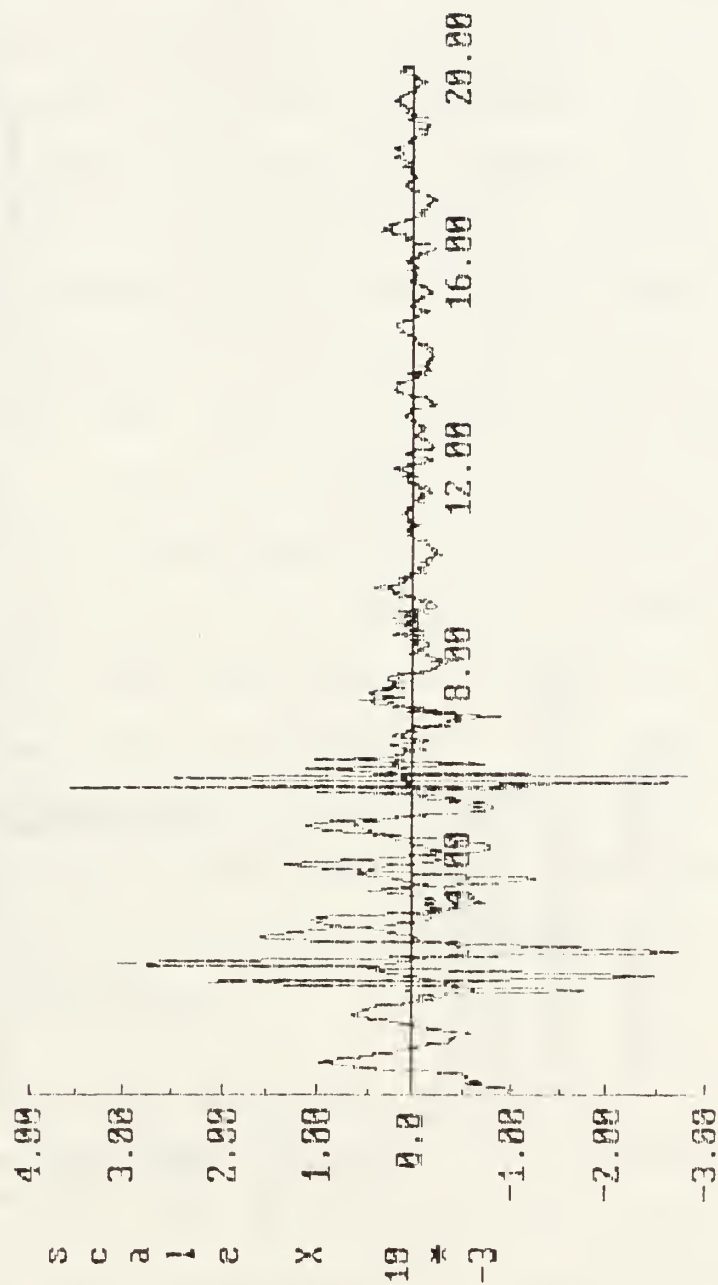
Figure 15. Overlay of target and background measurements

37

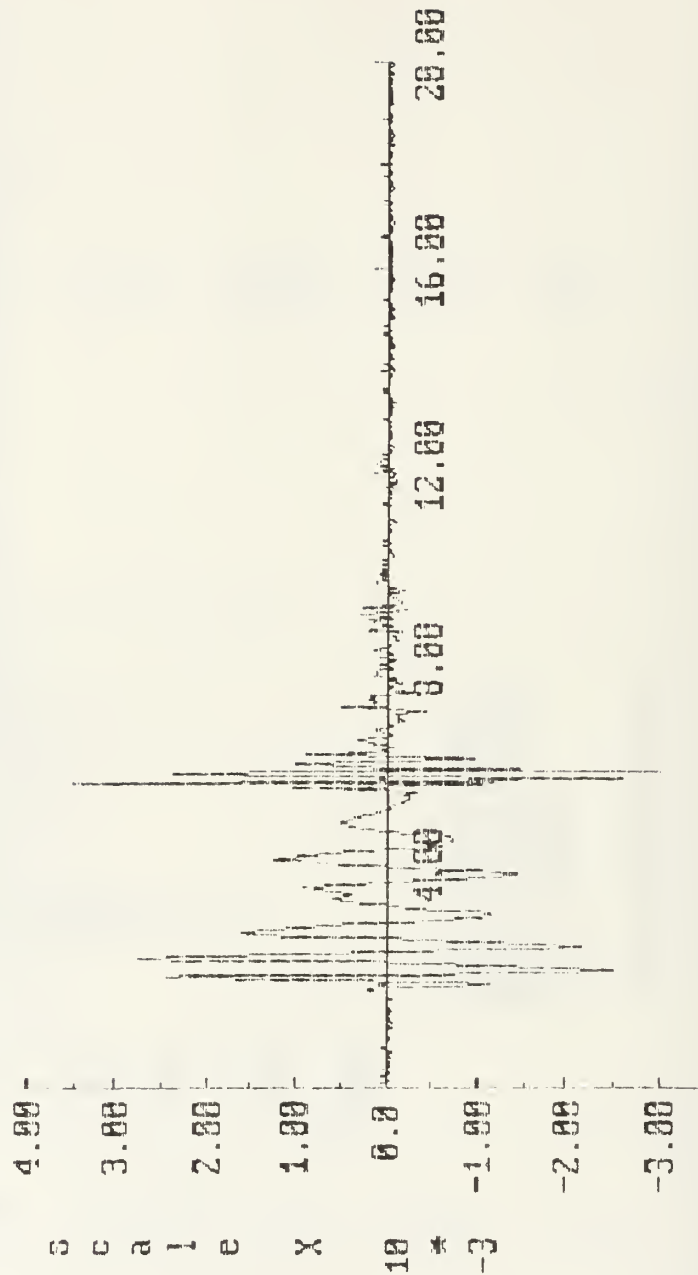Figure 16. Subtracted waveform

The three frequency-domain transforms, the FFTs of the numerically computed calibration sphere, the measured calibration shpere and the measured target response are then formed into Riad's optimal deconvelution estimator given in equation 3.6. The program then asks the operator for the smoothing parameter "C". This parameter is kept as small as possible to prevent oversmoothing and loss of spectral content. It was found that C = 0.009 gave good results and was used throughout this work. The frequency domain estimator formed by Raid's method yields a best approximation for the scattered signal produced by the same incident plane wave used for the computed calibration sphere. This frequency domain estimator is displayed to the operator. The program then transforms it into the time domain and the result is again displayed. The operator has the option of saving the deconvolution result, reprocessing with a different smoothing parameter, or processing another target.

B.   USE IN AMPLIFIER-ANTENNA DESIGN AND VALIDATION

In the example subtracted waveform, as presented in Figure 16, the residual system noise both before and after the scattered signal can be observed. This noise is random and has no apparent harmonic content. When trial measurements were first made with the new amplifier-antenna configuration, a seemingly harmonic content in the noise was

39

observed. This harmonic content was observed only in a target-subtracted waveform. It was not observed in the background waveform or when a background measurement was subtracted from another background waveform. It was concluded that the harmonic content could be from residual multi-path scattering between the metalized antenna mounting panel and the target. When the panel was masked, as can be seen in Figure 4, the harmonic content of the noise in the subtracted waveform disappeared.

The frequency domain estimator formed by the post-processing provided the first clue to another potential problem: possible destructive interference between the two pulses after the 6-12 GHz pulse had been delayed in time by pre-amplification. In Figure 17, a deep hole can be seen in the frequency domain estimator at roughly 5 GHz. When the raw data from the same measurement was transformed into the frequency domain, using an FFT, several nulls were observed in the area of spectral overlap between the two amplifiers. A number of trial measurements were made and the same observation was made in the FFT spectrum and in the frequency domain estimator between 5 and 6.5 GHz.

To confirm what was actually being transmitted into the chamber, each antenna lead was in turn disconnected and terminated through two 20 dB attenuators and a 50 ohm terminator. A series of scattering measurements were made
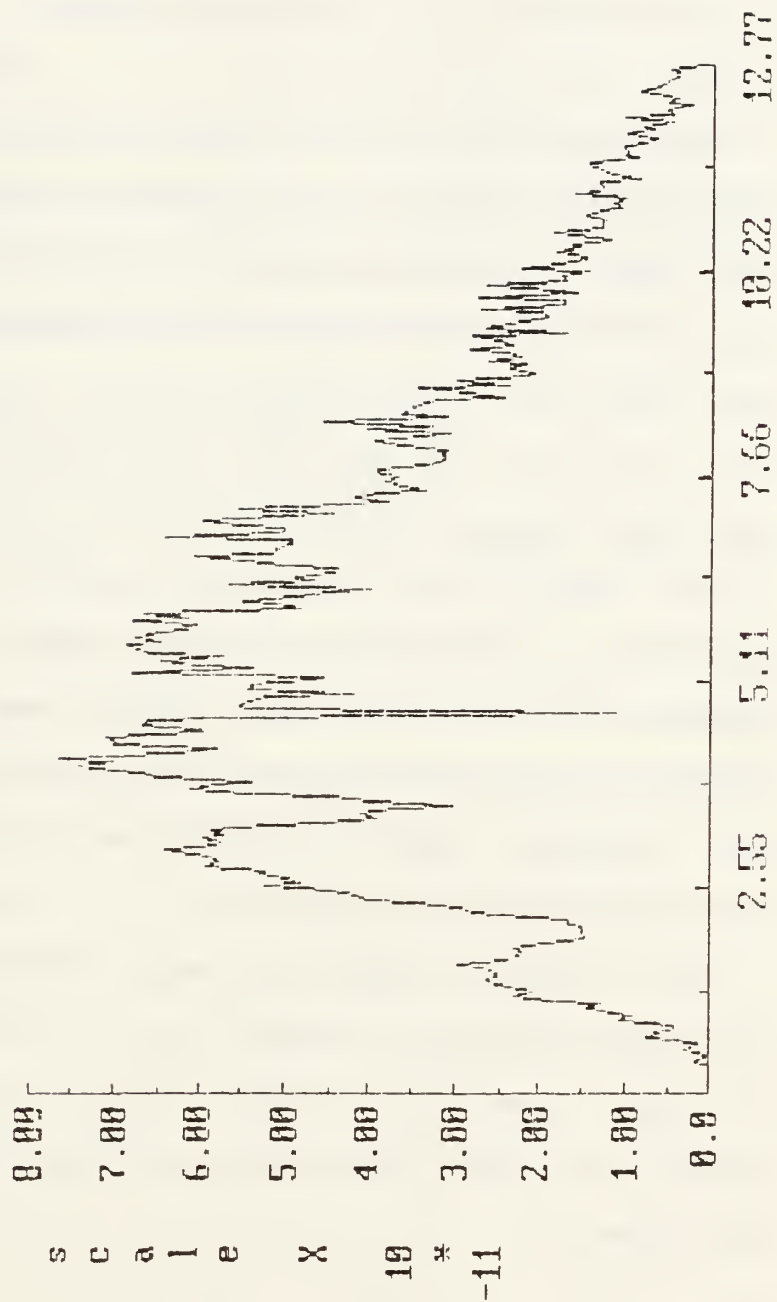
Figure 17. Frequency domain estimator with spectral hole

with each antenna terminated. These measurements were then processed using the deconvolution algorithm followed by FFT transformation. In all cases the spectral content from 5 to 6.5 GHz was found to be rich.

The deconvolution algorithm was also used to determine the length of delay line required to bring the two pulses into phase with each other at the receiving antenna. A number of trial measurements using different-sized spheres were made with each length of delay line. The measurement data was then put through the post-processing and the resulting frequency domain spectral estimator was compared to the theoretically predicted spectral plot. Each delay line was also lengthened by approximately 1 cm through the addition of a male-male and female-female 141 mil coaxial section. The measurements and subsequent processing were then repeated. Thus, by trial and error, the final delay line length was determined.

In the next chapter the deconvolution results for three different canonical targets will be presented. These were obtained using the final amplifier configuration. In addition, an SNR calculation based upon measurements will be considered.

V. SYSTEM VALIDATION

A. CANONICAL TARGETS

To validate the fidelity of the final equipment configuration the time domain results of the deconvolution program are compared with numerically generated waveforms for simple canonical targets. Three targets were used:

- A 12.28 centimeter diameter metal sphere,
- A 8.10 centimeter diameter metal sphere,
- A 10 centimeter long, 2.36 millimeter diameter thin wire.

Three programs, MIE, SPRSCT and TDIE-DG, written by Morgan [Ref. 2], were used to generate the theoretical waveforms for the targets. MIE computes the frequency domain magnitude and phase for the metallic spheres. These are then used as inputs to SPRSCT to compute the transient scattering response to the specified double-gaussian incident waveform.

TDIE-DG was used for the thin wire calculations. This program solves a time-domain integral equation to generate the induced current on the wire for a specified double-gaussian pulse incident plane wave field. The scattered field is then calculated by a numerical space-time integration using the induced currents. The input parameters for these programs are summarized in Table 4.

43

TABLE 4.   NUMERICAL COMPUTATION INPUTS

Sphere radius in meters, 12 cm sphere   0.061415

Sphere radius in meters, 8 cm sphere   0.04050

Bistatic angle in degrees   3.0

Scattering plane   E plane

Time window in ns   20

Narrow 10% pulse width in ns   0.15

Wide 10% pulse width in ns   0.30

Wire length in meters   0.10

Wire radius in meters   0.00118

Scattering angle in degrees   90

Scattering angle in degrees   45

The numerically generated theoretical waveform and the measured deconvolution waveform for the two spheres and the thin wire are overlaid in Figures 18, 19, 20 and 21. Thin wire results are presented for both 90 and 45 degree incidence angles. The time base has been shortened as compared to Figure 14 so that the detail can be examined. It can be seen that the agreement between the plots is excellent. The high level of fidelity of the TESL and the accuracy of the deconvolution algorithm are apparent from these overlays.

Some residual noise and clutter can be observed as a slight ripple on the measured waveforms. These signal pollutants appear to be less than what was seen in previous work. The system noise estimation presented in Reference 4 was repeated for comparative purposes and is presented in the next section.

B.   SYSTEM NOISE ESTIMATION

In order to compare the system signal-to-noise ratio to that calculated during previous work on the TESL [Refs. 3 & 4], the same thick wire target was again measured. This target is a 10 cm long, 5.2 mm diameter, copper wire. The measured response of this wire is shown in Figure 23. Two consecutive background measurements were also made for the purpose of the noise estimation. One background measurement was first subtracted from the target waveform. The
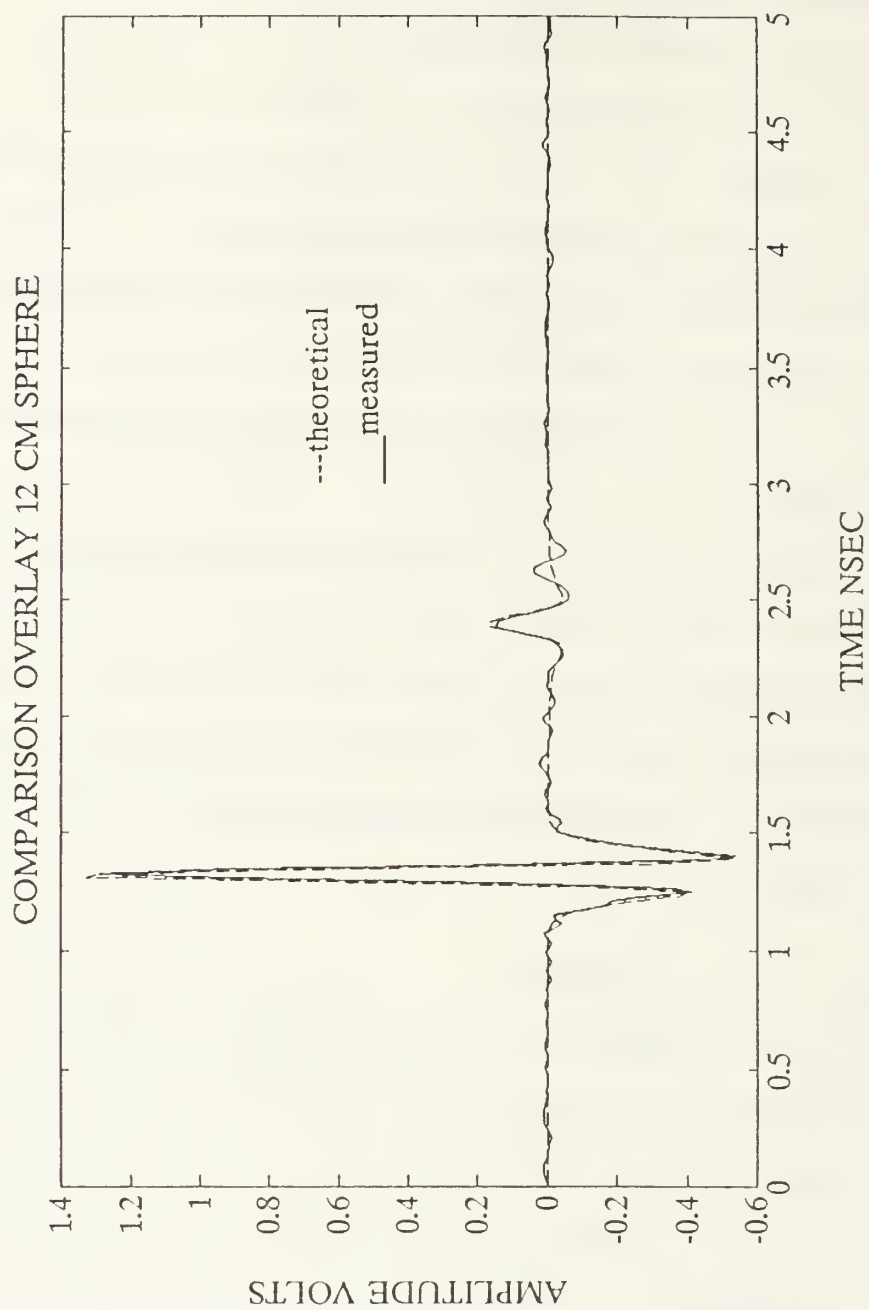
Figure 18. The 12.2 cm diameter sphere validation

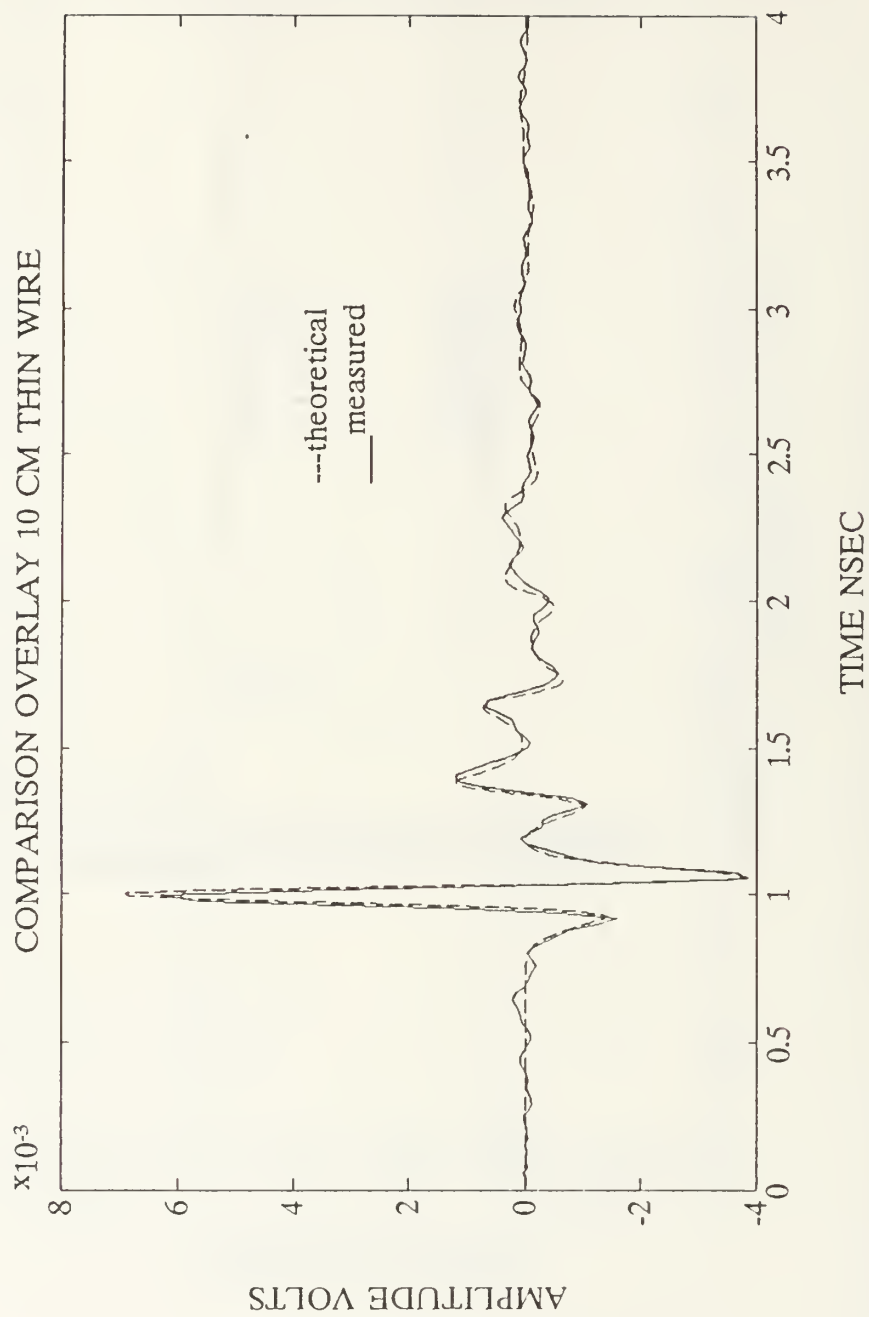Figure 19.   The 8.1 cm diameter sphere validation

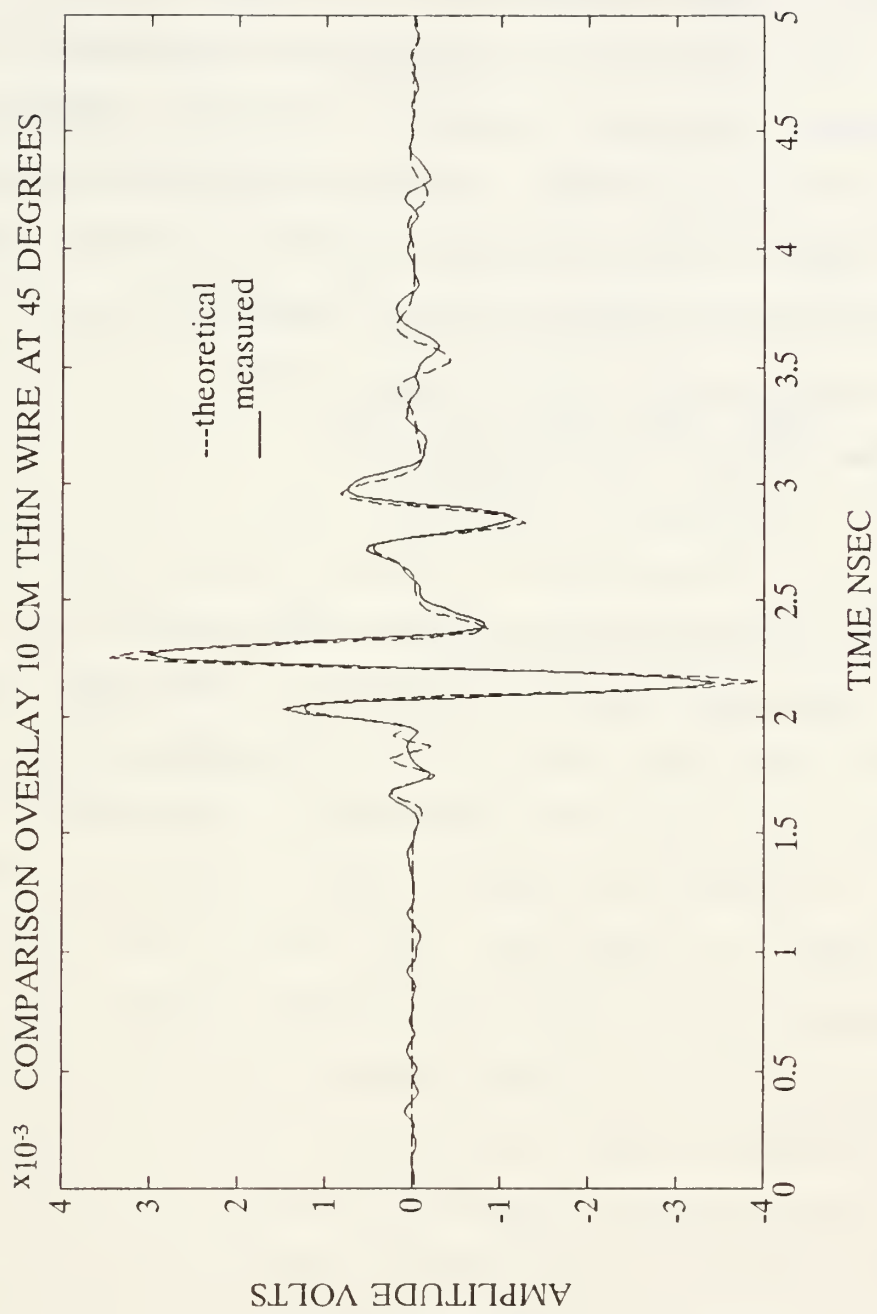Figure 20.   The 10 cm thin wire at 90 degrees validation

Figure 21.   The 10 cm thin wire at 45 degrees validation

subtracted signal waveform was then time-windowed to include only the signal duration. This time series is denoted by $x(t_n)$. The two consecutive background measurements were then subtracted from each other to eliminate chamber clutter. This record is denoted as $N(t_n)$. Statistical summaries of these two records are found in Tables 5 and 6. The signal-to-noise ratio (SNR) was then calculated as

$$SNR = \frac{\frac{1}{T_1}\left[(E_x - E_N)\right]}{\frac{1}{T_2}E_N} = \frac{\sum_n\left[x^2(t_n) - N^2(t_n)\right]}{\sum_n N^2(t_n)} \qquad (5.1)$$

The resulting SNR obtained using equation 5.1 was 26.6 dB. When this effort started, it had been expected to replace the one watt 1-6 GHz amplifier with a two watt device. The two watt amplifier is unavailable until 1990 and a further increase of SNR is expected when the new amplifier is installed. The thick wire measurement was repeated several times and similar results were obtained. Sompaee [Ref. 4] reported a SNR of 27.31 dB. When his target measurements were re-examined, it was found that the seemingly harmonic content of the noise existed, which lead to the masking of the antenna mounting panel in this work. Thus, his SNR may have been contaminated with a multi-path contribution which was eliminated during this work. As well, it was found that by allowing the amplifiers to reach

thermal stability before measurements were taken produced better results. For this work, the hardware was allowed to warm up for approximately two hours before measurements were taken. The SNR calculation was also repeated using the target waveforms discussed in the next chapter. Direct comparisons could then be made using the same target, same number of ensemble averages, and the same software used for the computations. These calculations demonstrated the improvement achieved in the SNR. Some target aspects demonstrated a very large response at frequencies greater than 7 GHz. These records showed an improvement in the SNR of up to 8 dB. In no cases examined was there a decrease in the SNR as compared to the target records from the single amplifier configuration.
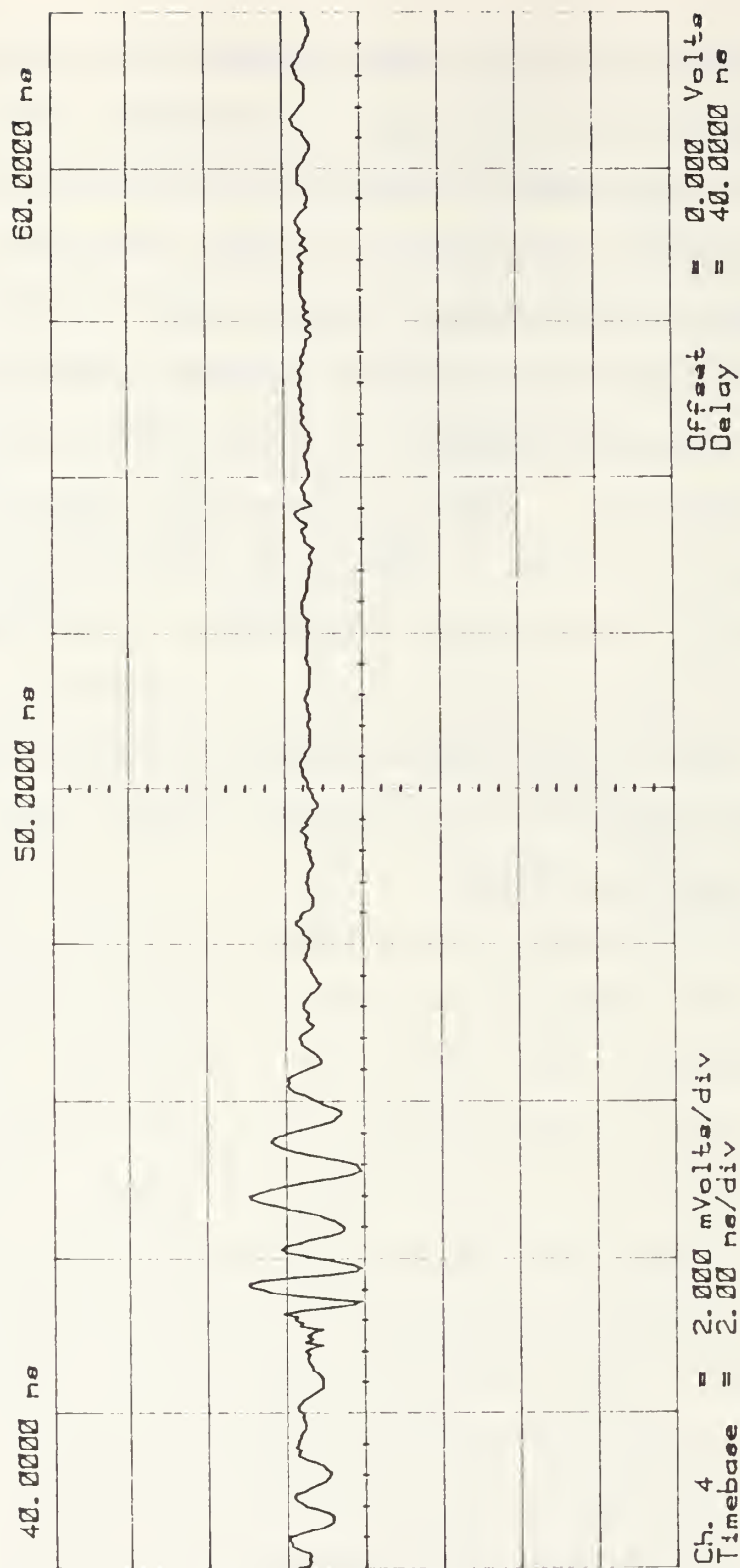
Figure 22. Thick wire signal plus noise waveform

52

TABLE 5. STATISTICS OF THICK WIRE SIGNAL PLUS NOISE
WAVEFORM

MEAN	3.4132E-5
STD DEVIATION	5.0376E-4
MEDIAN	3.6864E-5
MAXIMUM	1.4631E-3
MINIMUM	-1.7556E-3

TABLE 6. STATISTICS OF NOISE WAVEFORM

MEAN	1.40966E-09
STD DEVIATION	2.3524E-05
MEDIAN	9.5810E-06
MAXIMUM	7.2081 E-05
MINIMUM	5.2919E-05

VI.   TARGET LIBRARY

The fidelity of the parallel amplifier configuration was demonstrated using the simple canonical targets discussed in Chapter V. The scattering response of the canonical targets is numerically computable to a high level of accuracy. This is not the case for more complex scattering targets. A primary purpose of the NPS TESL is to support research into aspect-invariant radar target identification, based on natural resonances. To facilitate this research a library of measurements on scale model aircraft targets was assembled. Six 1/72 scale-model targets of military aircraft were selected. Each plastic model has been carefully coated with silver paint to excite a scaled transient scattering response, duplicating the aircraft modeled.

Each target file contains 14 measurements. Each measurement is constructed from 2048 ensembled averages of 1024 data points in a 20 ns window. The same measurements were made for each of the aircraft targets as follows:

- A calibration sphere measurement

- A background measurement

- Target measurement, 30 degrees from nose-on (30°)

- A second background measurement

- Target measurement, nose-on (0°)

- A third background measurement

- Target measurement, broadside (90°)

- A fourth background measurement

- Target measurement, tail-on (180°)

- A fifth background measurement

- A target measurement, viewed from the top with the wings horizontal

- A sixth background measurement

- A target measurement viewed from the top with the wings vertical

- A seventh background measurement.

It took roughly one hour to acquire each target waveform and its background pair. The DPO acquired the data in nine minutes per measurement, after which it took roughly 15 minutes for the IEEE 488 bus transfer to the computer. Hard copies of each target response were then made before proceeding to the next measurement. Figures 24 to 27 are examples of the waveforms obtained. Each has been time windowed from the original 20 ns record so detail can be seen. Table 7 lists the full-size dimensions of the aircraft modeled.

TABLE 7. FULL SIZE DIMENSIONS OF TARGETS RECORDED

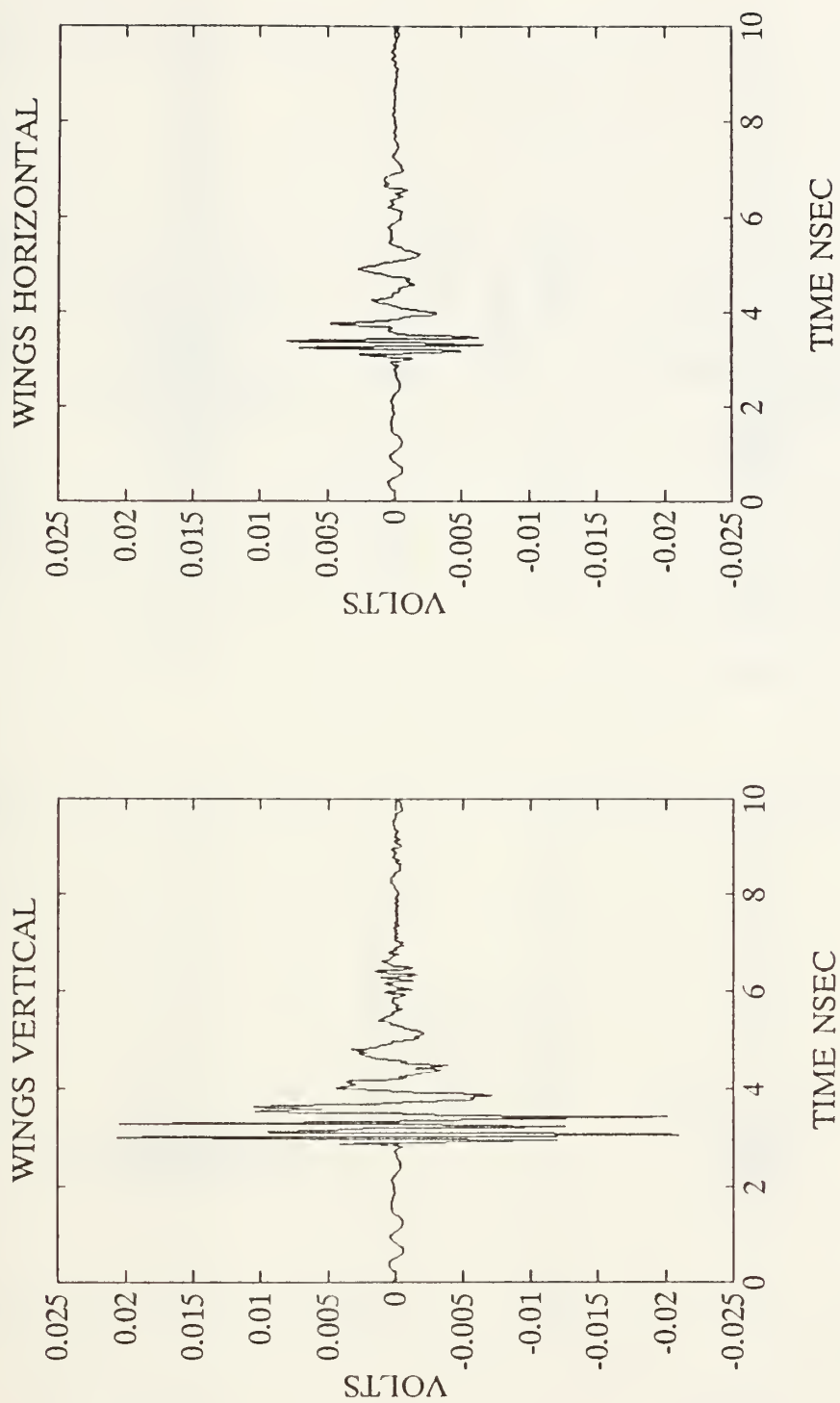| Target number	1	2	3	4	5	6
Overall length (meters)	12.20	16.00	19.43	16.94	15.03	20.81
Overall height (meters)	3.35	4.80	5.63	4.51	5.09	4.46
Wingspan (meters)	10.96	13.95	13.05	11.43	10.00	11.62
Tailplane span (meters)	unknown	5.75	8.61	6.92	5.58	N/A

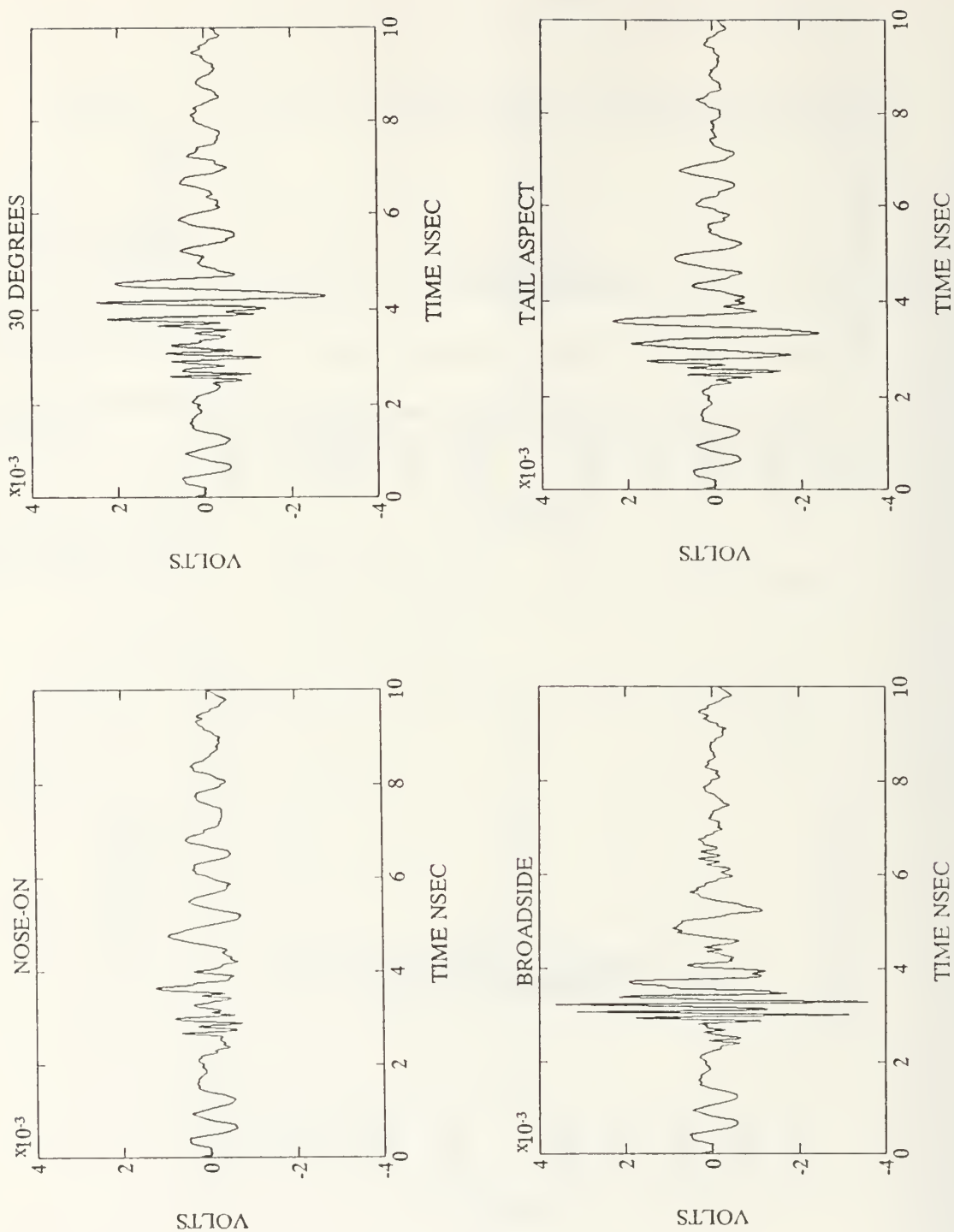Figure 23. Comparison of vertical and horizontal wing
oriented target 3 top view
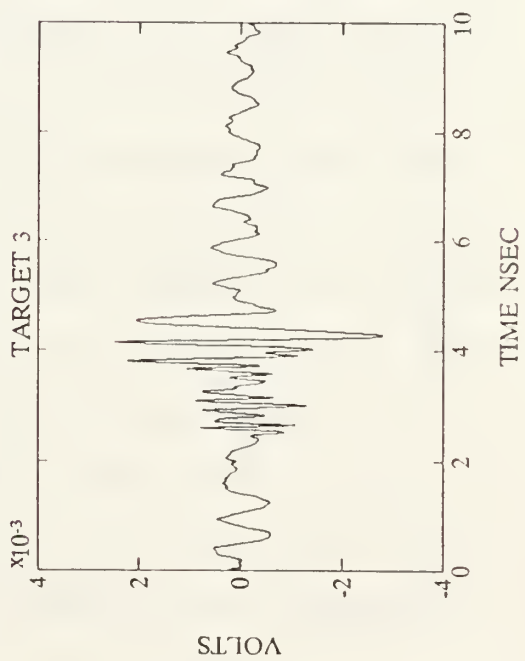
57

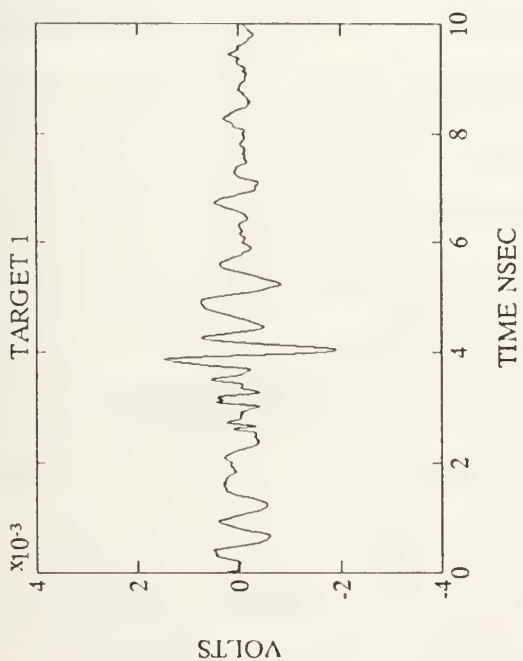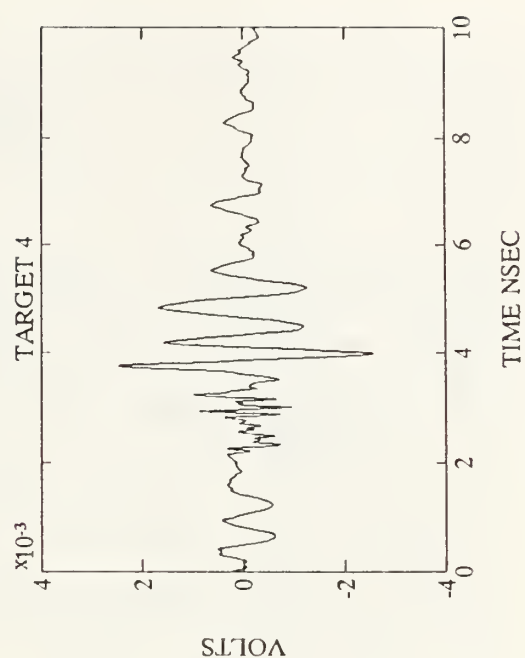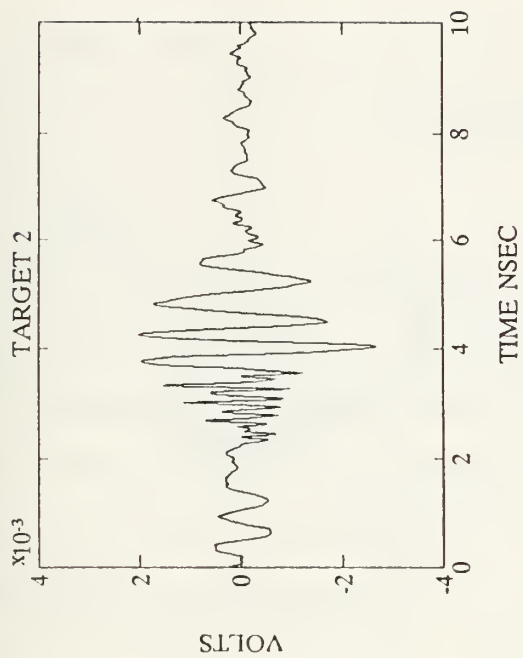Figure 24. Target 3 at 0, 30, 90 and 180 degree aspect angle

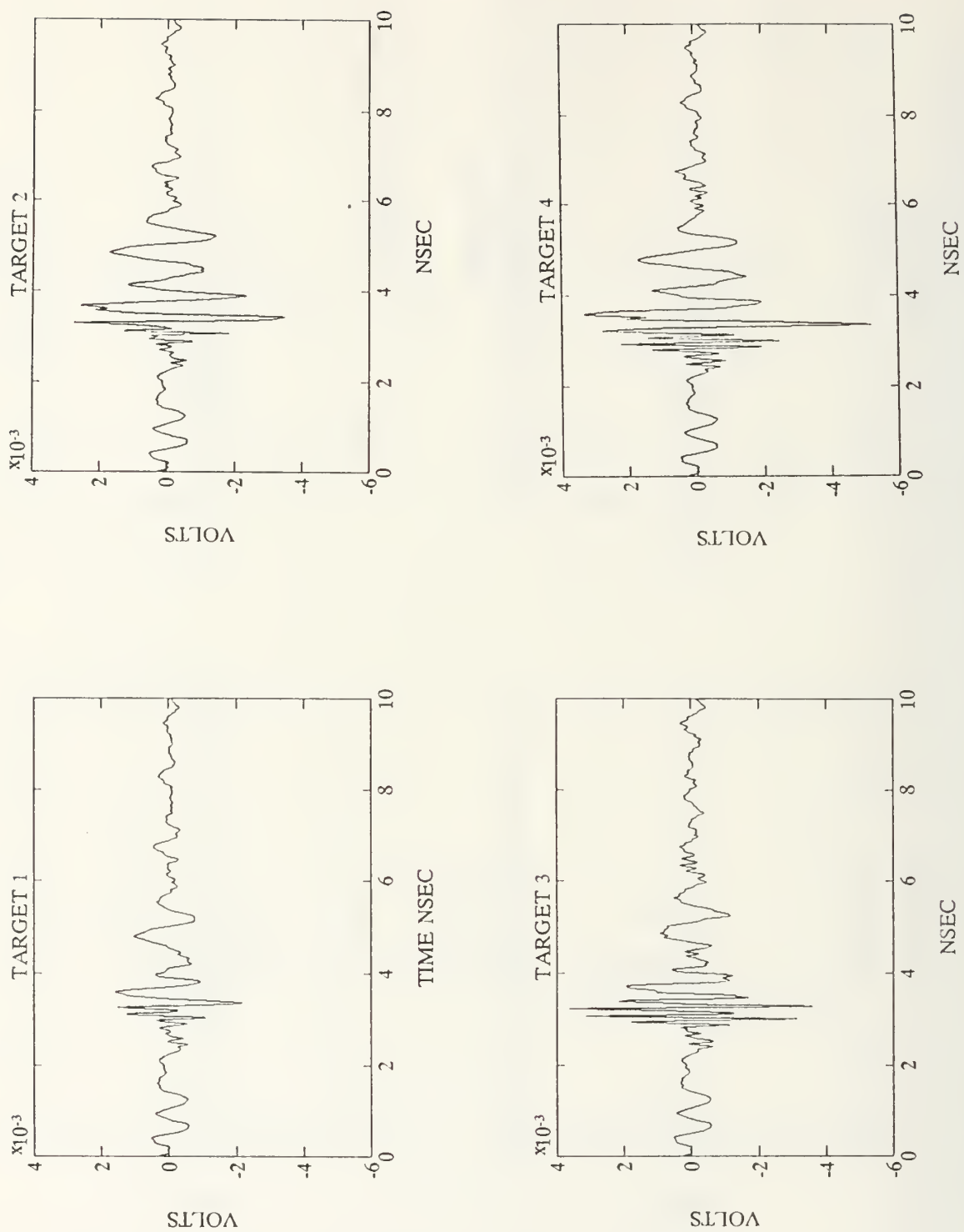Figure 25. Comparison targets 1, 2, 3, and 4 nose-on

59

Figure 26. Comparison targets 1, 2, 3, and 4 broadside

60

VII CONCLUSIONS

A. SUMMARY

The thrust of the effort described in this thesis has been the development, implementation and validation of a parallel amplifier configuration for the NPS TESL. The resultant increase in bandwidth and SNR will enhance the quality of the measurements taken to support a number of research applications. To support those efforts, an extensive library of high fidelity target measurements for both canonical and complex scattering targets was created.

The first stage of this effort was the development of the parallel amplifier configuration. The TESL software support system was used extensively in this development. A scalar network analyzer was used to characterize the new 6-12 GHz amplifier and the first parallel configuration tested led to frequency domain modeling of the relative magnitudes of the spectral content of the pulse generator from 1-12 GHz. This modeling lead to the preamplification of the 6-12 GHz amplifier which, in turn, lead to the delay of the 1-6 GHz pulse. The delay was required to eliminate destructive interference between the pulses caused by the time-delay introduced by the preamplification.

The parallel amplifier configuration was then validated by comparing the outputs of the deconvolution post-

61

processing for canonical targets to the numerically computed scattered waveforms due to a double-gaussian incident pulse. Very good agreement was shown, which attests to the accuracy of the experimental procedure and the deconvolution algorithm. A noise analysis was presented and the causes of the SNR improvement seen in the new hardware configuration were examined.

The final stage of this work was the creation of a high fidelity library of scattering responses for canonical and complex targets. The library has been described and example waveforms presented.

B.   FUTURE CONSIDERATIONS

In Chapter V, Section B, the prospect of further increasing the SNR by replacing the one watt 1-6 GHz amplifier was mentioned.   Other possible hardware improvements include the use of a matching two watt 6-12 GHz amplifier, should one become available.   In addition, the preamplifier currently employed could be replaced with a more compact low-noise device. This latter measure would facilitate rack mounting the time domain equipment, DPO, DC power supply, sampling front-end and amplifiers. This equipment could then be more readily removed and replaced with alternate hardware configurations for use in obtaining broadband scattering measurements.

Under consideration is the use of a more mature and more widely-used technique employing a stepped-frequency continuous wave system. It would use a network analyzer front-end as a coherent receiver. Frequency domain measurements could then be made and directly compared to the library compiled in the time domain.

LIST OF REFERENCES

1. C.W. Hammond, "The Development of a Bistatic Electromagnetic Scattering Laboratory", Master's Thesis, Naval Postgraduate School, Monterey, CA, 1980.

2. M.A. Mariatequi, "Development, Calibraogtion, and Evaluation of a Free Field Scattering Range", Master's Thesis, Naval Postgraduate School, Monterey, CA, 1983.

3. Brent W. McDaniel, "Calibration and Evaluation of a Free Field Scattering Range Using Wideband Pulse Amplification", Master's Thesis, Naval Postgraduate School, Monterey, CA, 1985.

4. Soonpuen Sompaee, "Computer Algorithms For Measurement Control and Signal Processing of Transient Scattering Signatures", Master's Thesis, Naval Postgraduate School, Monterey, CA, 1988.

5. Om P. Gandhi, <u>Microwave Engineering and Applications</u>, Pergamon Press, Maxwell House, Fairview Park, Elmsford, NY, 1988.

6. Merrill Skolnik, <u>Radar Handbook</u>, McGraw-Hill, Inc., NY, 1970.

7. <u>Encyclopedia of Polymer Science and Technology</u>, Volume 5, Intersciece Publishers, John Wiley & Sons, NY, 1966.

8. Suhner Coaxial Connectors General Catalog, 1988, Woburn, MA.

9. William H. Hayt Jr., <u>Engineering Electromagnetics</u>, 4th Edition, McGraw-Hill Inc, NY, 1981.

10. S. Lawrence Marple, <u>Digital Specral Analysis With Applications</u>, Prentice-Hall, Inc., Englewood Cliffs, N.J., 1987.

11. S.M. Raid, "Impulse Response Evaluation Using Frequency Domain Optimal Compensation Deconvolution", presented at the Midwest Symposium on Circuits and Systems, University of Toledo. OH, August 1981.

INITIAL DISTRIBUTION LIST

No. Copies

1. Defense Technical Information Center   2
   Cameron Station
   Alexandria, VA 22304-6145

2. Library, Code 0142   2
   Naval Postgraduate School
   Monterey, CA 93943-5002

3. Department Chairman, Code 62   1
   Department of Electrical and
   Computer Engineering
   Naval Postgraduate School
   Monterey, CA 93943-5100

4. Professor Michael A. Morgan, Code 62Mw   10
   Department of Electrical and
   Computer Engineering
   Naval Postgraduate School
   Monterey, CA 93942-5100

5. Professor Rama Janaswamy,Code 62Js   1
   Department of Electrical and
   Computer Engineering
   Naval Postgraduate School
   Monterey, CA 93942-5100

6. Dr. John N. Entzminger   1
   Director, Tactical Technology Office
   Defense Advanced Resesarch Projects Agency
   1400 Wilson Blvd.
   Arlington, VA 22209

7. Dr. Dominick Giglio   1
   Tactical Technology Office
   Defense Advanced Resesarch Projects Agency
   1400 Wilson Blvd.
   Arlington, VA 22209

8. Dr. Arthur Jordan   1
   Code 1114SE
   Office of Naval Research
   800 N.Quincy St.
   Arlington,VA 22209

9. Dr. Rabiner Madan   1
    Code 1114SE
    Office of Naval Research
    800 N.Quincy St.
    Arlington,VA 22209

                          .

10. Professor K. M. Chen   1
    Department of Electrical Engineering and
    Systems Science
    Michigan State University
    East Lansing, MI 48824

11. Dr. Michael L. Van Blaricum   1
    Toyon Corporation
    75 Aero Camino, Suite A
    Goleta, CA 93117

12. Mr. Daniel Carpenter   1
    TRW Military Electronics and Aviation Division
    One Rancho Carmel
    San Diego, CA 92128

13. Librarian   2
    National Defense Headquarters
    MGen George R. Pearkes Building
    Ottawa Canada K1A OK2

14. LCOL G. Hug   1
    DLR3
    Directorate Land Requirements
    National Defense Headquarters
    MGen George R. Pearkes Building
    Ottawa, Canada K1A OK2

15. Maj N.J. Walsh   5
    c/o DLAEEM4
    Directorate of Land Armaments
    Electronics Engineering and Maintenance
    National Defense Headquarters
    MGen George R. Pearkes Building
    Ottawa, Canada K1A OK2